JOURNAL OF PETROLOGY | VOLUME 44 | NUMBER 1 | PAGES 55–91 | 2003

Petrogenesis of Cenozoic Basalts from Mongolia: Evidence for the Role of Asthenospheric versus Metasomatized Lithospheric Mantle Sources

T. L. BARRY[1]*, A. D. SAUNDERS[1], P. D. KEMPTON[2], B. F. WINDLEY[1], M. S. PRINGLE[3], D. DORJNAMJAA[4] AND S. SAANDAR[4]

[1]GEOLOGY DEPARTMENT, UNIVERSITY OF LEICESTER, UNIVERSITY ROAD, LEICESTER LE1 7RH, UK

[2]NERC ISOTOPE GEOSCIENCES LABORATORY, KEYWORTH NG12 5GG, UK

[3]SUERC/NSS AR FACILITY, SCOTTISH ENTERPRISE TECHNOLOGY PARK, EAST KILBRIDE G75 0QF, UK

[4]CENTRE OF PALAEONTOLOGY, MONGOLIAN ACADEMY OF SCIENCES, ULAAN BAATAR—210613, PO BOX 863, MONGOLIA

RECEIVED AUGUST 14, 2000; REVISED TYPESCRIPT ACCEPTED JULY 10, 2002

Diffuse Cenozoic volcanism in Mongolia forms part of a widespread tectono-magmatic province that extends from NE China to Lake Baikal, Siberia. Mafic lavas from the Gobi Altai, southern Mongolia (~33 Ma) and Hangai, central Mongolia (<6 Ma) have remarkably similar trace element characteristics, with light rare earth element enrichment (La_n/Yb_n = 11·2–46·6) and positive K, Nb and Sr anomalies on mantle-normalized trace element diagrams. On the basis of new crustal xenolith data, it can be demonstrated that the basalts have not experienced significant crustal contamination. Trace element and Sr–Nd–Pb–Hf isotopic data suggest that these magmas originated by partial melting of a heterogeneous metasomatized amphibole-bearing garnet peridotite mantle source at depths >70 km. Three isotopic end-members can explain the heterogeneity: (1) is similar to bulk silicate Earth with $^{206}Pb/^{204}Pb$ >~17·8 and is asthenospheric; (2) is EM1-like, characterized by low $^{206}Pb/^{204}Pb$ (>17·062), and may represent mobilized ancient lithospheric mantle; (3) also lithospheric, is characterized by low $^{143}Nd/^{144}Nd$ (>0·512292) and shows similarities to EM2, although decoupling of isotopic systems suggests a complex enrichment process. The timing of lithospheric enrichment is unconstrained, but may be related to Mesozoic magmatic events and/or melts mobilized during the Cenozoic responding to higher than ambient potential temperature mantle. Published geophysical studies suggest anomalous material at the base of the lithospheric mantle; however, there is no evidence to suggest a high heat flux mantle plume. Volcanism is likely to occur where localized extensional conditions are favourable.

KEY WORDS: *argon dating; basalts; xenoliths; mantle metasomatism; modelling; Mongolia*

INTRODUCTION

Cenozoic intraplate volcanism in Mongolia is diffuse and widespread but generally small in volume; individual volcanic provinces typically comprise <30 km^3 of magmatic rocks. Numerous models have been proposed to explain the petrogenesis of these magmas, including: (1) a mantle plume or hotspot (e.g. Logatchev, 1984; Zorin & Lepina, 1985; Windley & Allen, 1993); (2) a crustal weakness along the Amur plate margin, which extends from the northern tip of Lake Baikal to the Pacific coast (Yarmolyuk *et al.*, 1991); (3) the combined effect of collision between India and Asia during the Eocene with secondary input from a mantle plume (Khain, 1990); (4)

*Corresponding author. Present address: BAS/NIGL, BGS, Keyworth NG12 5GG, UK. Telephone: +44 (0) 115 9363191. Fax: +44 (0) 115 9363302. E-mail: tbarry@bgs.ac.uk

thermal blanketing caused by collision of continental plates (Petit *et al.*, 2002). In the absence of evidence for sufficient regional extensional tectonics to explain the magmatism, i.e. extension greater than a β value of two (McKenzie & Bickle, 1988), most explanations have favoured a model involving a mantle plume. It should be noted that although small-scale extension is contemporaneous with magmatism in some parts of Mongolia (e.g. Tariat), the amount of lithospheric thinning is insufficient to be the cause of magmatism. However, a number of lines of evidence appear to be inconsistent with the presence of a substantial, deep-rooted mantle plume. These are: (1) the diffuse nature of the volcanism; (2) the lack of age progression within the volcanic provinces; (3) the small volumes of intermittent magmatism throughout the Cenozoic; (4) the lack of mantle xenolith evidence for lithospheric temperatures in excess of 1100°C (Ionov *et al.*, 1998); (5) the absence of geophysical evidence for a deep upwelling of mantle but instead growing evidence for anomalous density material between 100 and 200 km (Petit *et al.*, 2002), which is coincidental with a low-velocity zone <220 km as determined by shear-velocity models (Villaseñor *et al.*, 2001); (6) the absence of high heat flow, only values around 50–60 mW/m^2 (Khutorskoy & Yarmolyuk, 1989; compare Windley & Allen, 1993); (7) the lack of a flood basalt province. Therefore we suggest that the presence of a mantle plume such as Hawaii or Iceland, or a start-up plume as inferred for some large igneous provinces (e.g. Campbell & Griffiths, 1990), is not evident beneath Mongolia.

For clarification, the definition of a mantle plume, as considered in this paper, is a thermally buoyant upwelling of lower- or upper-mantle material that originates from a thermal boundary layer, such as the D" layer or 670 km discontinuity. A mantle plume should have an anomalously high potential temperature and definable spatial boundaries, and should generate magmas with distinctive chemical signatures. It should be noted that a thermal anomaly alone is insufficient evidence to distinguish a mantle plume—this may simply mean that the asthenospheric mantle has a higher than ambient potential temperature, which could reflect the presence of mantle material that has been emplaced laterally or vertically in response to tectonic stresses, or as a result of thermal blanketing of the underlying asthenosphere (see Anderson *et al.*, 1992). We aim to shed new light on whether the volcanism in Mongolia is a consequence of an actively upwelling mantle plume or a passive process related to tectonic stresses.

Regardless of which process caused the magmatism, we investigate the petrogenesis of the Mongolian volcanic rocks by determining the relative contributions to the parent magmas from asthenospheric and lithospheric mantle sources. Numerous workers have proposed lithospheric contributions to intraplate basaltic magmatism (e.g. Kempton *et al.*, 1991; Wilson & Downes, 1991; Class *et al.*, 1998; Zhang *et al.*, 1999). However, Arndt & Christensen (1992) have suggested that conductive heating of anhydrous lithosphere cannot explain significant volumes of melt generation, suggesting that the lithospheric mantle must be metasomatically or volatile enriched.

To address these questions we focus on two regions of basaltic volcanism in Mongolia. The first is Hangai (Fig. 1b and c), a domally uplifted area of central Mongolia attributed to mantle upwelling (Windley & Allen, 1993). The second area is the Gobi Altai (Fig. 1b and d), which is located south of Hangai, and potentially includes the earliest Cenozoic volcanic activity in Mongolia. The aims of this study are: (1) to constrain the processes involved in magma genesis; (2) to determine the composition of the mantle source regions, and identify any contribution from the lithospheric mantle in the formation of the magmas; (3) to assess whether or not a mantle plume has been involved in the petrogenesis of the Mongolian Cenozoic magmas.

GEOLOGICAL SETTING AND STRATIGRAPHIC RELATIONSHIPS

Widespread diffuse alkalic volcanism has occurred throughout much of Asia since the Miocene (e.g. Whitford-Stark, 1987). From southern China, through the extension-related basins of NE China to the Baikal rift, there are occurrences of small-volume basaltic magmatism (Fig. 1a). Regardless of spatial and temporal differences, the chemistry of the rocks remains remarkably similar (e.g. Barry & Kent, 1998). The volcanic rocks have exhumed a range of mantle and crustal xenoliths (e.g. Ionov *et al.*, 1992, 1994, 1995; Tatsumoto *et al.*, 1992; Wiechert *et al.*, 1997), which provide good constraints on the nature of the underlying lithosphere.

Mongolia occupies a unique position within the broad Asian tectono-magmatic province. It has been the focus of several major studies of strain dissipation within the crust as a consequence of the India–Asia collision (e.g. Tapponnier & Molnar, 1979; Cobbold & Davy, 1988). Mongolian basement geology comprises a mosaic of Precambrian continental blocks, Palaeozoic arc terranes and Mesozoic sedimentary basins (see summaries by Buchan *et al.*, 2001; Cunningham, 2001).

Hangai, central Mongolia

The Hangai region has been described as 'domed' (e.g. Windley & Allen, 1993; Cunningham, 2001). It is a mountainous region covering >200 000 km^2 with numerous flat-topped peaks over 3000 m (e.g. Cunningham,

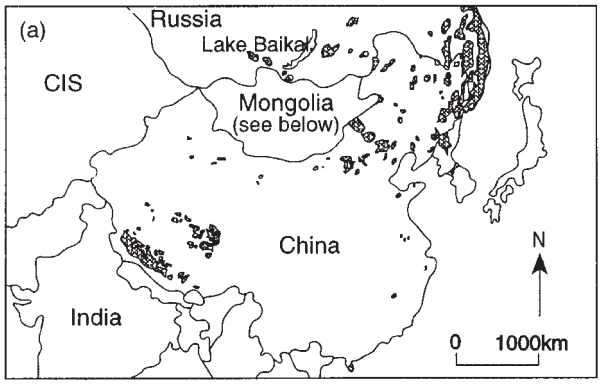

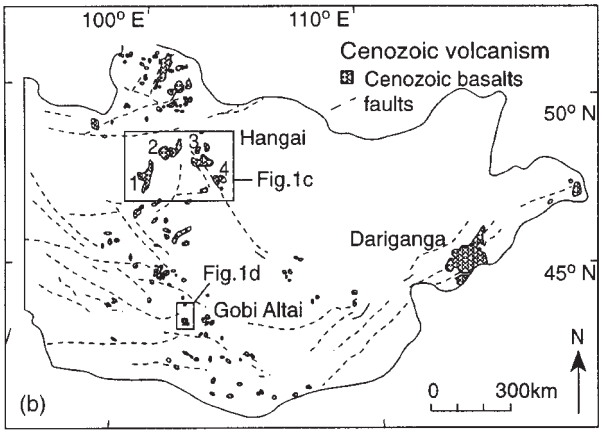

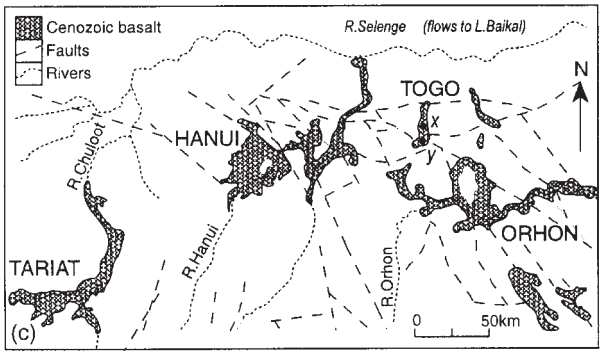

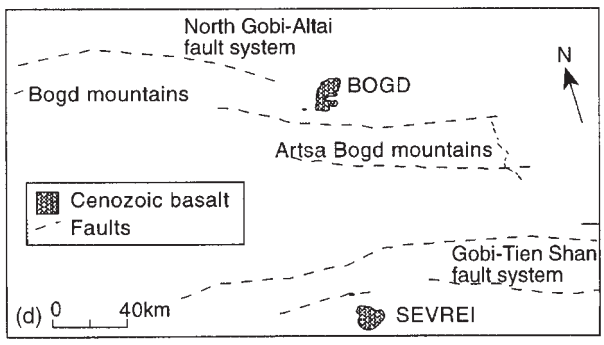

2001). On the basis of the presence of tilted sediments, uplift and doming began in the middle Oligocene (Devyatkin, 1975; Barsbold & Dorjnamjaa, 1993), reaching a maximum uplift of 2 km (Devyatkin, 1975). The Hangai region represents an important kinematic link between the Baikal rift province to the north and the Altai transpressional ranges to the south and west (e.g. Cunningham, 2001). Late Cenozoic uplift of the southern part of Hangai appears to be confined to an area underlain by cratonic basement, whereas the Altai region to the south and west, including the Gobi Altai, is underlain by mechanically weaker Palaeozoic arc and accretionary belts (Cunningham, 2001).

Numerous small volcanic provinces are distributed throughout the Hangai area, of which the four most northerly ones are studied here: Tariat, Hanui, Togo and Orhon (Fig. 1c). A brief summary of the setting of these volcanic fields is given below. A summary of the petrographic characteristics of the lava types from each locality, including typical phenocryst assemblages, degree of alteration and presence or absence of xenoliths, is presented in Table 1. Most of the lavas are olivine $\pm$ clinopyroxene phyric with many of the phenocrysts displaying skeletal structures or forming a glomeroporphyritic texture. The rocks are not significantly altered, except for the matrix glass, but some samples show iddingsitization of olivine and more rarely sericitization of plagioclase (Table 1).

The Tariat volcanic province (55 km $\times$ $\sim$12 km; Fig. 1c) has been the subject of several detailed studies of mantle (e.g. Preß *et al.*, 1986; Stosch *et al.*, 1986; Ionov *et al.*, 1998) and crustal (Kopylova *et al.*, 1995; Stosch *et al.*, 1995) xenoliths. Within Mongolia, the Tariat province is exceptional for its xenolith abundance. At this locality, steeply incised river canyons cut through sequences of flat-lying lavas (up to 20 m thick); individual lavas within these sequences are commonly $\sim$8–12 m thick. Basement rocks are exposed in the valley walls, and although their age is unknown they are inferred to be Precambrian to Carboniferous in age.

Field relationships indicate that the youngest lavas lie within half-grabens that now form the present-day river channels; older lavas occur high on the uplifted valley sides, indicating that uplift has occurred throughout the period of volcanism. In this context, the lava sequences are similar to some basalt volcanic fields in the Basin

Fig. 1. (a) Regional distribution of Cenozoic volcanism throughout Russia and China (based on Whitford-Stark, 1987; Fan & Hooper, 1989; Lysak, 1995). (b) Distribution of Cenozoic volcanism throughout Mongolia [(adapted from Barry & Kent (1998)]. Numbers relate to individual volcanic provinces: 1, Tariat; 2, Hanui; 3, Togo; 4, Orhon. (c) Map of Hangai volcanic provinces (*x*, Ikh Togo Uul; *y*, Baga Togo Uul). (d) Map of Gobi Altai volcanic provinces and their relation to regional fault systems.

Table 1: Representative petrographic descriptions for volcanic provinces and formations from Hangai and Gobi Altai

Volcanic province	Rock type	Normative classification	Phenocryst			% estimates of ground mass phases						Groundmass %		Presence of: 1, Xenoliths 2, Xenocrysts
			Mineral	%	(mm)	plag	ol	cpx	cpx*	opq	other	size (mm)	alteration	
Tariat–Sumyn Formation														
	PT	ne-norm.	ol	7–12	0·4	22	13	6	—	2	glass; 50	0·2	glass; 100%	1, Mantle; 2, Ol
Tariat–Chuluut Formation														
	B	hy-norm.	ol	2	<1	49	21	6	—	3	glass; 19	<0·5	—	—
	TB	ne- to hy-norm.	ol†	5	1	19	26	13	—	2	glass; 34	0·3	glass; 100%	2, Ol
	BTA	hy-norm.	ol	18	1·5	59	—	16	—	2	—	0·05	—	1, Mantle; 2, Ol
	BA	qtz-norm.	ol†	2	2	21	16	3	—	—	glass; 51	0·3	glass; 100%	—
	PT	hy-norm.	ol†	3	1·6	18	16	13	—	2	glass; 35	0·4	glass; 100%	—
Tariat–Morun Formation														
	BTA	hy-norm.	cpx‡ + ol	23	1	32	—	19	—	11	—	<0·3	—	—
Tariat–Goramsan Formation														
	TB	ne-norm.	ol + cpx‡	2	1	32	22	17	—	18	idd; 10	0·05	—	—
	TeB	ne-norm.	ol	7	0·7	47	15	—	24	7	—	0·2	—	—
	F	ne-norm.	ol + cpx	13	0·4	—	—	—	—	—	—	<0·01	—	—
Hanui	BTA	ne- to hy-norm.	ol	2	0·9	51	8	6		3	vesicles	0·3	—	—
	PT	ne-norm.	ol	3	0·4	52	25	—	16	4	—	—	idd; 10%	—
Togo	TeB	ne-norm.	ol	5	0·5	45	12	—	28	6	—	<0·2	—	1, Mantle; 2, Ilmenite
	BTA	ne-norm.	ol (+ plag)	18	<0·4	—	—	—	—	—	glass	<0·01	—	2-Ol
	PT	ne-norm.	ol (+ cpx‡)	23	0·8	9	—	—	—	—	glass	<0·01	glass; 100%	1, Mantle
Orhon	BTA	ne- to hy-norm.	ol‡	22	<2·2	42	9	—	15	12	—	0·1	idd; 10%	1, Mantle (altered)
Gobi Altai–Bogd														
	BTA	ne-norm.	—	—	—	53	25	—	3	2	—	0·3	sericite; 5%	1, Mantle and crustal
	TA	ne-norm.	ol	3	1	43	30	—	7	5	—	<0·1	—	2, Ilmenite
Gobi Altai–Sevrei														
	BTA	ne-norm.	ol	7	1	49	9	—	13	13	—	<0·1	idd; 80%	—

B, basalt; BA, basaltic andesite; TB, trachybasalt (hawaiite); BTA, basaltic trachyandesite (mugearite); TA, trachyandesite (benmoreite); PT, phonotephrite; TeB, tephrite basanite; F, foidite; TeP, tephri-phonolite; ne, nepheline; hy, hypersthene; qtz, quartz; ol, olivine; cpx, clinopyroxene; opq, opaque minerals; idd, iddingsite.
*Small stubby cpx.
†Skeletal crystal structure.
‡Glomeroporphyritic texture.

and Range province of the western USA (Kempton *et al.*, 1987). On the basis of field relationships and geographical locality, the Tariat lavas can be divided into four formations that range in age from late Miocene to Recent (Barry, 1999). From oldest to youngest these are the Goramsan, the Morun, the Chuloot and the Sumyn Formations. For completeness, we provide information on the formation from which particular samples have been taken in Tables 1–3, but for the purpose of this geochemical study, the volcanic rocks from Tariat will be considered as part of a single province.

Other basalt volcanic provinces within the Hangai area include Hanui, Togo and Orhon. Hanui is a flat-lying volcanic plain, some 120 km NE of Tariat, covering an area of 3500 km^2 (Fig. 1c). Fifty kilometres due east of Hanui is the Togo province (Fig. 1c), a flat plain with two volcanic centres: Ikh Togo Uul (literal translation 'great Togo mountain') and Baga Togo Uul ('big Togo mountain'). Baga Togo Uul consists of three vents, one of which is maar-like. Both volcanic centres are covered in vegetation, but some trench excavations on Ikh Togo Uul expose scoria, volcanic bombs and lava. Basalt from Baga Togo Uul is rich in ilmenite megacrysts (<1 cm) and altered peridotite xenoliths. The Orhon province comprises a section of lavas of 50 m thickness to the SE of Togo (Fig. 1c). Individual basalt lavas are 10–15 m thick with columnar jointing towards the top.

Eastern Gobi Altai

The Gobi Altai is located ~300 km south of Hangai. The area is dissected by strike-slip faulting and the volcanic fields lie in close proximity to two major left-lateral transpressional faults: the North Gobi–Altai Fault System in the north and the Gobi–Tien Shan Fault System in the south (Fig. 1d; Cunningham *et al.*, 1997). The faulting is a far-field expression of the collision between India and Asia, which occurred ~55 Myr ago (Tapponnier & Molnar, 1979; Cunningham *et al.*, 1997; Cunningham, 2001). Whether the faults were active at the time of volcanism is at present unknown. The basalts form solitary plateaux of near-horizontal lavas. The Bogd Plateau, in the north, covers ~100 km^2, a similar area to the Sevrei Plateau, 150 km to the south (Fig. 1d).

The Bogd Plateau consists of at least five individual lavas, each 8–12 m thick. The lavas have oxidized upper surfaces with ropy texture, and the thicker lavas exhibit columnar jointing. Many of the lavas contain crustal and/or mantle xenoliths. The Sevrei Plateau, like the Bogd Plateau, is a remnant of a once larger edifice, as shown by erosional scarps of vertical columnar joints at the sides of the plateaux, rather than rubbly lava.

SAMPLING STRATEGY AND ANALYTICAL TECHNIQUES

Samples of all the fresh mafic rock exposed within the study areas were collected during two separate field seasons. The rocks were collected to sample as wide a diversity of temporal, spatial and chemical variation as possible. Xenoliths, both crustal and mantle, were collected along with their host rock whenever encountered.

A total of 66 whole-rock samples were crushed in a fly press and finely powdered in an agate Tema swing mill. Major elements were determined on fusion beads made from pre-ignited rock powders fused with lithium metaborate flux in a ratio of 1:5. Trace elements Nb, Zr, Y, Sr, Rb, Ga, Zn, Ni, Sc, V, Cr, Cu and Ba were analysed on powder pellets. Both major and trace elements were analysed at the University of Leicester by X-ray fluorescence (XRF) spectrometry using an ARL 8420 wavelength-dispersive system fitted with a Rh anode X-ray tube and a Philips PW1400 spectrometer with a W anode tube. Representative data are reported in Table 3, and the complete dataset may be downloaded from the *Journal of Petrology* website at http://www.petrology.oupjournals.org.

La, Ce, Pr, Nd, Sm, Eu, Gd, Tb, Dy, Ho, Er, Tm, Yb, Lu, Pb, Th and U concentrations were determined by instrumental neutron activation analysis (INAA) at the University of Leicester and by inductively coupled plasma mass spectrometry (ICP-MS) at Cardiff University or at the NERC ICP-MS facility, Silwood Park, Ascot. Analytical techniques for INAA analyses at Leicester (including sample preparation, conditions of sample counting and detector resolution) have been described by Fitton *et al.* (1998). Samples for ICP-MS analysis (Cardiff and Silwood Park) were prepared using a standard HF–HNO_3 digestion. Drift and background were monitored by analysing international standards BIR (Cardiff) and JB-1 (Silwood Park); a blank was run after every five unknowns.

Thirteen crustal xenoliths [four collected by T.L.B. and nine provided by H.-G. Stosch (see Stosch *et al.*, 1995)] were analysed for major elements by ICP atomic emission spectrometry (ICP-AES) at the University of Leicester, following the sample preparation procedure described in the Appendix. The elements Th, Nb, Rb, Pb, Zr, Hf, Y, La, Ce, Pr, Nd, Sm, Eu, Gd, Tb, Dy, Ho, Er, Tm, Yb and Lu were analysed by ICP-MS at the NERC facility, Silwood Park, and monitored using the procedures described for the whole-rock samples.

Sr, Pb, Nd and Hf isotope compositions were analysed as metal species on single Ta, single Re, double Re–Ta and double Re–Re filaments, respectively, using a Finnegan MAT 262 multicollector mass spectrometer at the NERC Isotope Geosciences Laboratory (NIGL). All

Table 2: Summary of Ar–Ar age data for samples from Tariat (Hangai) and Gobi Altai

Sample	Latitude, longitude	Rock type	Age spectra							Isochron		
			Total gas age (Ma)	Increments (°C)	Number of steps	K/Ca	% ^{39}Ar	Weighted age (Ma)	MSWD	Age (Ma)	^{40}Ar/^{36}Ar intercept	Sums/(N − 2)
Hangai (Tariat)												
Chuluut Formation												
MN-10.1.1	48°13′N, 100°26′E	TB	0·57 ± 0·01	440–1300	8 of 9	0·92	97·5	0·53 ± 0·02	6·81	0·55 ± 0·02	294·1 ± 3·0	9·49
Morun Formation												
MN-11.2.2	48°13′N, 100°26′E	BTA	5·88 ± 0·02	440–1300	6 of 12	1·20	74·6	5·91 ± 0·018	3·18	5·91 ± 0·02	295·4 ± 6·1	4·10
Eastern Gobi Altai												
Bogd												
TB95-2.10	44°41′N, 102°13′E	BTA	30·5 ± 0·1	440–1300	16 of 21	2·07	83·4	30·4 ± 0·1	1·80	30·3 ± 0·1	325·5 ± 8·3	1·00
Sevrei												
TB95-12.2	43°31′N, 102°11′E	BTA	33·0 ± 0·1	440–1300	10 of 20	1·11	50·3	33·0 ± 0·1	3·00	33·0 ± 0·3	285·4 ± 36·9	3·50
TB95-12.7.2	43°30′N, 102°10′E	BTA	32·8 ± 0·1	440–1300	12 of 20	0·96	78·0	32·7 ± 0·2	26·60	32·4 ± 0·4	309·4 ± 31·6	31·7

The ^{40}Ar/^{36}Ar intercept value for TB95-2.10 is slightly high at 325·5 ± 8·3, and could be due to recoil during irradiation, giving old ages at low-temperature steps and a young age at high-temperature steps. These steps have not been included in the plateau age. Lithological abbreviations are the same as in Table 1.

Table 3: Geochemical data for a representative set of Cenozoic Mongolian volcanic rocks

	Tariat–Sumyn Formation		Tariat–Chuloot Formation				
Sample no.:	MN-5.3.1	MN-12.2	MN-3.5	MN-5.2.2	MN-8.4.1	MN-9.1.3	MN-10.1.1
Latitude (N):	48°13·78′	48°13·75′	48°12·73′	48°13′	48°13·21′	48°13·75′	48°13·05′
Longitude (E):	100°26·38′	100°26·42′	100°26·14	100°26′	100°25·55′	100°26·42′	100°26·40′
Lithology:	PT	PT	BTA	B	BA	TB	TB
SiO_2	49·09	48·74	49·77	49·53	53·81	50·41	50·14
Al_2O_3	15·10	14·89	15·11	14·88	15·70	15·18	15·34
Fe_2O_3	11·15	11·14	11·21	11·19	9·76	10·69	11·39
MgO	8·03	8·00	7·68	8·45	6·05	7·77	7·46
K_2O	3·97	3·92	3·06	2·19	1·96	2·44	2·99
Na_2O	3·51	3·43	3·13	2·51	3·16	3·01	3·06
CaO	6·63	6·78	6·91	8·18	7·49	8·11	7·11
TiO_2	1·86	1·93	1·83	1·98	1·71	1·90	1·73
MnO	0·15	0·15	0·15	0·16	0·14	0·15	0·16
P_2O_5	0·96	0·97	0·77	0·58	0·51	0·66	0·76
Total	100·46	99·95	99·61	99·65	100·30	100·33	100·14
LOI	−0·46	−0·51	−0·22	0·65	−0·23	−0·03	−0·28
Mg-no.	61·82	61·75	60·64	62·93	58·22	62·04	59·56
Rb*	45	45	46	27	24	36	39
Ba*	615	635	530	479	362	597	545
Th†	4·56	4·58	4·03	2·45	2·54	2·91	3·98
U†	1·24	1·24	1·26	0·89	0·57	0·76	1·01
Nb*	58·1	58·9	48·9	40·0	29·6	44·0	42·8
Ta	—	—	2·80	2·46	1·70	2·70	2·63
La†	56·05	56·30	43·48	23·99	23·45	31·40	42·06
Ce†	106·16	105·66	82·88	49·37	47·77	63·15	80·31
Pb†	6·46	6·51	5·71	2·87	4·24	4·61	5·65
Pr†	12·36	12·26	9·86	6·30	6·02	7·68	9·62
Sr*	1047	1064	931	713	617	979	873
Nd†	47·85	46·93	37·54	26·36	24·79	29·95	37·16
Sm†	8·66	8·74	7·40	5·77	5·68	6·37	7·32
Zr*	297	299	281	180	186	218	247
Hf	5·98	6·61	6·36	4·53	4·44	5·53	6·14
Eu†	2·82	2·80	2·49	1·97	1·93	2·14	2·40
Gd†	7·76	7·73	6·58	5·43	5·30	5·99	6·76
Tb†	0·97	0·97	0·86	0·76	0·75	0·81	0·86
Dy†	4·61	4·61	4·31	3·91	3·87	4·18	4·36
Y*	20	20	20	19	19	20	19
Ho†	0·71	0·73	0·70	0·65	0·65	0·71	0·71
Er†	1·73	1·73	1·69	1·62	1·69	1·76	1·74
Tm†	0·21	0·20	0·21	0·22	0·21	0·23	0·21
Yb†	1·13	1·21	1·23	1·18	1·22	1·29	1·27
Lu†	0·16	0·15	0·17	0·17	0·17	0·19	0·18
Ni*	175	172	160	140	84	125	139
Cr*	233	225	201	188	142	169	192
ne	6·4	6·2	0·1	0·0	0·0	0·0	0·0
di	11·0	11·6	9·5	11·6	9·2	12·7	9·4
q	0·0	0·0	0·0	0·0	2·1	0·0	0·0
ol	18·9	18·6	19·0	11·0	0·0	13·9	17·4
hy	0·0	0·0	0·0	11·5	20·4	4·8	2·0
$^{87}Sr/^{86}Sr$	0·704694	—	0·704796	0·704314	0·704763	0·705304	0·704864
$^{143}Nd/^{144}Nd$	0·512555	—	0·512555	0·512705	0·512635	0·512646	0·512556
εNd	−1·62	—	−1·62	1·31	−0·06	0·16	−1·60
$^{206}Pb/^{204}Pb$	17·0620	—	17·2220	17·8010	17·7300	17·5080	17·2350
$^{207}Pb/^{204}Pb$	15·4640	—	15·4750	15·4860	15·4870	15·4740	15·4750
$^{208}Pb/^{204}Pb$	37·1750	—	37·3180	37·7580	37·7000	37·5040	37·3240
$^{176}Hf/^{177}Hf$	0·282736	—	0·282713	0·282952	—	—	—
εHf	−1·27	—	−2·08	6·38	—	—	—

Table 3: continued

	Tariat–Chuloot Formation						
Sample no.:	MN-12.1.2	MN-13.2	MN-13.5	MN-14.1	MN-16.2	MN-16.2.1	MN-16.2.2
Latitude (N):	48°13·75′	48°14·07′	48°13·27′	48°12·83′	48°12·44′	48°13·75′	48°13·75′N
Longitude (E):	100°26·42′	100°23·04′	100°21·82′	100°22·16′	100°24·42′	100°26·42′	100°26·42′
Lithology:	BTA	TB	BTA	TB	TB	TB	BTA
SiO_2	52·22	50·10	52·27	51·70	49·26	50·30	51·43
Al_2O_3	15·18	15·24	15·86	15·69	15·02	15·27	15·08
Fe_2O_3	10·49	10·76	9·80	10·38	11·02	10·82	10·64
MgO	6·98	6·94	5·84	6·38	7·21	7·65	7·65
K_2O	2·06	2·59	2·45	2·57	3·13	2·98	2·36
Na_2O	2·95	3·40	3·25	2·84	4·43	2·94	3·03
CaO	7·54	7·77	7·57	7·89	7·11	7·62	7·55
TiO_2	1·79	1·97	1·89	1·86	1·98	1·77	1·72
MnO	0·15	0·15	0·14	0·15	0·15	0·15	0·15
P_2O_5	0·55	0·73	0·64	0·68	0·69	0·76	0·60
Total	99·90	99·66	99·70	100·16	100·02	100·27	100·23
LOI	−0·43	−0·42	−0·17	0·84	0·13	−0·10	−0·29
Mg-no.	59·94	59·19	57·26	58·02	59·53	61·39	61·78
Rb*	29	39	38	34	44	47	33
Ba*	436	633	563	589	593	622	555
Th†	2·73	3·20	2·36	3·06	4·31	4·02	2·78
U†	0·66	0·82	0·36	0·87	1·09	1·03	0·69
Nb*	33·7	48·9	40·2	41·1	51·0	53·4	36·3
Ta	—	—	—	—	—	2·87	—
La†	25·33	33·19	22·00	30·79	38·71	37·20	28·11
Ce†	52·01	66·23	45·65	60·73	74·67	71·41	56·07
Pb†	4·07	4·98	3·42	4·51	5·68	5·18	4·60
Pr†	6·46	8·03	5·86	7·48	8·90	8·60	6·74
Sr*	682	871	820	811	1015	979	763
Nd†	26·48	31·62	24·59	30·09	34·52	34·06	27·15
Sm†	5·83	6·82	5·67	6·27	6·81	6·60	5·70
Zr*	187	241	241	220	261	263	204
Hf	—	—	—	—	—	5·71	—
Eu†	2·00	2·28	1·84	2·12	2·27	2·23	1·93
Gd†	5·50	6·37	5·11	5·87	6·10	6·16	5·40
Tb†	0·78	0·85	0·75	0·82	0·82	0·80	0·75
Dy†	4·05	4·32	3·71	4·08	4·07	4·02	3·94
Y*	20	22	20	20	18	19	20
Ho†	0·70	0·74	0·64	0·68	0·67	0·66	0·63
Er†	1·72	1·76	1·53	1·74	1·63	1·57	1·56
Tm†	0·22	0·22	0·20	0·22	0·20	0·21	0·20
Yb†	1·31	1·32	1·20	1·30	1·17	1·22	1·20
Lu†	0·17	0·17	0·16	0·18	0·16	0·16	0·17
Ni*	85	106	69	90	101	131	143
Cr*	136	136	103	164	132	146	152
ne	0·0	0·4	0·0	0·0	0·8	0·0	0·0
di	9·8	12·7	10·1	10·3	11·4	11·1	10·9
q	0·0	0·0	0·0	0·0	0·0	0·0	0·0
ol	0·7	15·9	2·8	3·7	17·5	16·4	9·1
hy	22·4	0·0	15·4	16·2	0·0	2·3	12·3
$^{87}Sr/^{86}Sr$	—	—	—	—	—	0·704599	—
$^{143}Nd/^{144}Nd$	—	—	—	—	—	0·512614	—
εNd	—	—	—	—	—	−0·47	—
$^{206}Pb/^{204}Pb$	—	—	—	—	—	17·4290	—
$^{207}Pb/^{204}Pb$	—	—	—	—	—	15·4830	—
$^{208}Pb/^{204}Pb$	—	—	—	—	—	37·4580	—
$^{176}Hf/^{177}Hf$	—	—	—	—	—	—	—
εHf	—	—	—	—	—	—	—

	Tariat	Tariat–Morun Formation			Tariat–Goramsan Formation		
Sample no.:	MN-22.5	MN-11.2	MN-11.2.1	MN-11.2.2	MN-15.1	MN-15.1.1	MN-15.2
Latitude (N):	48°06·02′	48°16·50′	48°13·75′	48°13·75′	48°10·20′	48°13·75′	48°09·90′
Longitude (E):	099°56·34′	100°28·75′	100°26·42′	100°26·42′	100°26·25′	100°26·42′	100°27·41′
Lithology:		BTA	BTA	BTA	TB	TeB	F
SiO_2	50·71	51·67	51·67	51·65	47·62	46·77	43·52
Al_2O_3	15·00	15·84	15·87	15·86	15·06	14·63	14·03
Fe_2O_3	10·78	10·12	9·81	10·16	11·26	11·35	12·64
MgO	7·74	6·19	6·33	6·55	8·59	9·27	7·57
K_2O	2·63	2·55	2·63	2·61	2·99	3·01	4·11
Na_2O	3·12	3·11	3·03	2·96	3·31	3·31	4·96
CaO	7·64	7·37	7·40	7·35	8·35	8·14	8·41
TiO_2	1·85	1·96	2·02	2·03	2·04	2·09	2·88
MnO	0·15	0·14	0·13	0·14	0·17	0·17	0·21
P_2O_5	0·66	0·69	0·69	0·70	0·91	0·94	1·53
Total	100·29	99·63	99·58	100·01	100·30	99·68	99·87
LOI	−0·34	0·01	0·34	0·19	0·28	0·28	0·23
Mg-no.	61·75	57·90	59·20	59·18	63·17	64·74	57·53
Rb*	45	34	34	32	50	48	69
Ba*	637	541	515	521	744	705	881
Th†	3·4§	2·62	2·57	2·59	4·54	4·50	6·11
U†	—	0·69	0·75	0·61	1·16	1·15	1·5
Nb*	46·4	44·8	46·4	43·3	67·1	68·3	93·0
Ta	2·48	—	—	—	—	—	—
La†	29·57§	26·57	26·27	26·36	44·20	46·15	81·22
Ce†	57·47§	55·44	55·68	55·28	85·10	87·43	152·84
Pb†	4·21§	3·63	3·54	3·38	5·18	4·64	6·48
Pr†	6·97§	7·24	7·28	7·14	10·40	10·52	17·89
Sr*	987	819	787	806	947	950	1457
Nd†	28·58§	30·56	31·17	30·88	39·87	40·33	67·17
Sm†	6·01§	6·86	6·97	6·71	8·08	7·98	12·78
Zr*	235	210	212	202	302	300	354
Hf	5·20	—	—	4·46§	6·15§	—	—
Eu†	1·96§	2·38	2·32	2·24	2·68	2·66	4·04
Gd†	5·54§	6·18	6·16	6·14	7·33	7·50	11·21
Tb†	0·73§	0·84	0·85	0·82	1·00	1·00	1·39
Dy†	3·57§	4·16	3·90	3·99	5·11	5·08	6·50
Y*	21	18	18	18	25	24	24
Ho†	0·66§	0·64	0·65	0·67	0·84	0·85	0·98
Er†	1·60§	1·55	1·47	1·51	2·02	2·06	2·10
Tm†	0·22§	0·19	0·18	0·18	0·26	0·25	0·24
Yb†	1·32§	1·09	1·08	1·09	1·51	1·48	1·25
Lu†	0·19	0·15	0·15	0·15	0·21	0·19	0·16
Ni*	136	87	88	94	150	188	100
Cr*	179	144	167	155	185	217	108
ne	0·0	0·0	0·0	0·0	6·6	7·7	22·7
di	12·1	8·8	8·7	8·2	15·1	15·1	23·5
q	0·0	0·0	0·0	0·0	0·0	0·0	0·0
ol	14·7	4·4	4·1	4·3	18·4	19·6	13·9
hy	4·2	15·0	15·3	16·3	0·0	0·0	0·0
$^{87}Sr/^{86}Sr$	0·705251	—	—	0·704458	0·704307	—	—
$^{143}Nd/^{144}Nd$	0·512614	—	—	0·512702	0·512714	—	—
εNd	−0·47	—	—	1·25	1·48	—	—
$^{206}Pb/^{204}Pb$	17·4800	—	—	17·8080	17·4480	—	—
$^{207}Pb/^{204}Pb$	15·4720	—	—	15·4670	15·4620	—	—
$^{208}Pb/^{204}Pb$	35·5070	—	—	37·7260	37·4170	—	—
$^{176}Hf/^{177}Hf$	0·282782	—	—	0·282992	0·282900	—	—
εHf	0·36	—	—	7·89	4·76	—	—

Table 3: continued

	Hanui							
Sample no.:	MN-24.1	MN-25.1	MN-25.2.5	MN-25.4	MN-25.5	MN-26.5	MN-26.10	MN-26.11
Latitude (N):	48°41·55′	48°49·65′	48°49·65′	48°49·65′	48°49·65′	48°56·91′	48°56·91′	48°56·91′
Longitude (E):	101°30·21′	101°44·70′	101°44·77′	101°44·77′	101°44·77′	102°07·97′	102°07·97′	102°07·97′
Lithology:	TB	BTA	BTA	BTA	BTA	BTA	BTA	PT
SiO_2	49·62	52·38	52·17	51·69	52·96	52·49	52·88	45·31
Al_2O_3	14·51	15·52	15·13	15·44	15·40	15·72	15·16	14·17
Fe_2O_3	10·67	10·14	10·16	9·62	9·94	9·70	9·44	11·62
MgO	7·17	5·53	6·83	4·85	5·75	4·74	5·25	7·70
K_2O	2·18	2·29	2·10	3·31	1·76	3·34	2·67	4·20
Na_2O	3·81	4·08	4·22	4·48	4·29	4·62	4·82	5·01
CaO	7·27	7·05	7·20	6·19	7·35	6·30	6·06	7·47
TiO_2	2·38	2·07	1·94	2·71	2·15	2·77	2·67	3·11
MnO	0·13	0·13	0·13	0·11	0·13	0·11	0·11	0·15
P_2O_5	0·64	0·59	0·51	0·84	0·49	0·86	0·83	1·40
Total	98·38	99·76	100·38	99·24	100·21	100·66	99·88	100·13
LOI	0·01	−0·36	−0·06	−0·29	−0·07	0·14	−0·4	−0·24
Mg-no.	60·17	55·08	60·18	53·13	56·53	52·35	55·56	59·84
Rb*	24	23	31	22	20	33	30	35
Ba*	369	358	460	369	351	466	462	466
Th†	1·76	1·55	3·00	1·53	1·45	1·78	1·76	1·72
U†	0·57	0·21	0·65	0·17	0·38	0·30	0·55	0·52
Nb*	48·0	39·3	33·0	37·5	35·0	62·6	58·0	59·3
Ta	—	2·07	—	—	—	—	—	—
La†	22·87	18·98	24·67	18·82	16·72	27·95	27·71	26·46
Ce†	47·91	42·33	50·23	41·04	37·19	61·55	61·55	57·87
Pb†	2·41	2·70	4·70	2·86	2·71	2·80	2·71	2·74
Pr†	6·54	5·76	6·37	5·68	5·13	8·43	8·46	8·22
Sr*	725	711	687	691	582	951	847	951
Nd†	28·26	25·27	25·80	24·89	22·44	36·90	36·99	35·81
Sm†	6·46	6·13	5·57	6·18	5·55	8·06	8·04	7·66
Zr*	212	190	200	194	169	254	230	248
Hf	—	4·63	—	—	—	—	—	—
Eu†	2·18	2·17	1·97	2·15	1·95	2·64	2·65	2·64
Gd†	6·00	5·85	5·28	5·73	5·23	6·94	6·87	6·68
Tb†	0·85	0·81	0·77	0·83	0·74	0·93	0·89	0·88
Dy†	4·30	4·21	4·02	4·13	3·77	4·37	4·39	4·17
Y*	23	20	19	20	17	20	21	19
Ho†	0·69	0·67	0·68	0·66	0·62	0·69	0·68	0·63
Er†	1·62	1·54	1·61	1·55	1·47	1·56	1·52	1·49
Tm†	0·21	0·19	0·21	0·19	0·19	0·19	0·19	0·17
Yb†	1·13	1·00	1·23	1·07	1·07	1·11	0·98	0·96
Lu†	0·16	0·14	0·18	0·14	0·15	0·14	0·13	0·14
Ni*	93	89	89	85	94	101	101	97
Cr*	173	130	151	127	169	111	127	112
ne	0·8	0·0	0·1	2·5	0·0	2·8	0·6	20·9
di	13·2	11·6	13·5	11·0	13·1	11·4	10·8	20·3
q	0·0	0·0	0·0	0·0	0·0	0·0	0·0	0·0
ol	15·5	9·0	14·9	10·7	7·0	10·4	11·4	14·0
hy	0·0	5·4	0·0	0·0	7·7	0·0	0·0	0·0
$^{87}Sr/^{86}Sr$	—	0·704071	—	—	—	—	—	—
$^{143}Nd/^{144}Nd$	—	0·512756	—	—	—	—	—	—
εNd	—	2·30	—	—	—	—	—	—
$^{206}Pb/^{204}Pb$	—	17·8770	—	—	—	—	—	—
$^{207}Pb/^{204}Pb$	—	15·4550	—	—	—	—	—	—
$^{208}Pb/^{204}Pb$	—	37·6950	—	—	—	—	—	—
$^{176}Hf/^{177}Hf$	—	—	—	—	—	—	—	—
εHf	—	—	—	—	—	—	—	—

	Togo					Orhon	
Sample no.:	MN-27.1	MN-27.3.1	MN-27.4	MN-28.2	MN-28.4	MN-30.2	MN-30.3
Latitude (N):	48°55·34′	48°55·34′	48°55·34′	48°59·53′	48°55·79′	48°34·52′	48°34·52′
Longitude (E):	102°45·75′	102°45·75′	102°45·75′	102°44·48′	102°46·22′	103°08·42′	103°08·42′
Lithology:	TeB	TeB	BTA	PT	PT	PT	BTA
SiO_2	45·11	44·94	50·23	47·73	46·72	49·51	50·67
Al_2O_3	12·43	12·47	14·39	14·44	13·36	14·05	14·06
Fe_2O_3	11·68	11·73	10·19	10·63	10·67	10·59	10·41
MgO	10·87	10·99	6·49	7·49	9·74	7·04	6·51
K_2O	3·16	3·27	4·01	2·97	3·41	3·52	3·11
Na_2O	4·98	4·84	3·58	4·83	5·09	4·20	4·15
CaO	7·36	7·53	7·64	7·17	6·57	7·62	7·55
TiO_2	3·06	3·07	2·87	2·74	2·63	2·17	2·81
MnO	0·14	0·14	0·14	0·13	0·14	0·13	0·13
P_2O_5	1·26	1·25	1·01	1·19	1·25	0·89	1·02
Total	100·04	100·25	100·55	99·32	99·57	99·75	100·41
LOI	−0·10	0·11	0·39	−0·23	−0·21	−0·23	0·64
Mg-no.	67·66	67·81	58·88	61·30	67·24	59·92	58·44
Rb*	46	49	51	37	46	46	36
Ba*	627	652	686	492	574	806	763
Th†	3·53	3·48	3·75	2·66	3·75	2·68	2·61
U†	0·85	0·94	0·95	0·74	1·04	0·48	0·63
Nb*	109·0	109·0	121·0	87·0	109·0	77·6	76·0
Ta	—	—	2·81	—	—	—	—
La†	46·88	47·00	49·70	38·93	46·76	35·69	36·77
Ce†	98·83	98·92	104·73	85·40	98·57	76·32	78·87
Pb†	2·26	2·27	2·65	2·48	3·11	2·69	2·83
Pr†	13·39	13·33	14·09	11·38	13·21	10·22	10·83
Sr*	1171	1192	1394	1112	1176	1232	1182
Nd†	56·37	56·35	57·99	49·41	55·43	43·48Nd	44·88
Sm†	11·27	11·10	11·90	9·96	11·09	8·72	9·02
Zr*	266	263	307	248	280	243	234
Hf	—	—	6·19	—	—	—	—
Eu†	3·53	3·63	3·70	3·19	3·51	2·78	2·99
Gd†	9·36	9·37	9·69	8·52	9·00	7·42	7·62
Tb†	1·16	1·16	1·23	1·05	1·12	0·93	0·96
Dy†	5·42	5·59	5·57	5·04	5·50	4·38	4·54
Y*	25	22	25	24	22	20	21
Ho†	0·80	0·80	0·84	0·78	0·79	0·68	0·70
Er†	1·75	1·66	1·87	1·72	1·70	1·48	1·56
Tm†	0·20	0·21	0·21	0·19	0·20	0·19	0·18
Yb†	1·06	1·08	1·17	1·15	1·11	1·02	1·02
Lu†	0·13	0·13	0·15	0·16	0·14	0·14	0·14
Ni*	312	332	160	151	294	120	124
Cr*	389	412	169	189	365	153	179
ne	19·0	19·2	5·1	11·4	16·4	8·9	4·2
di	21·6	22·0	16·7	15·9	17·5	19·1	17·0
q	0·0	0·0	0·0	0·0	0·0	0·0	0·0
ol	19·3	19·4	12·0	14·7	18·3	13·4	12·2
hy	0·0	0·0	0·0	0·0	0·0	0·0	0·0
$^{87}Sr/^{86}Sr$	—	—	0·703995	—	—	—	—
$^{143}Nd/^{144}Nd$	—	—	0·512536	—	—	—	—
εNd	—	—	−1·99	—	—	—	—
$^{206}Pb/^{204}Pb$	—	—	17·8860	—	—	—	—
$^{207}Pb/^{204}Pb$	—	—	15·4500	—	—	—	—
$^{208}Pb/^{204}Pb$	—	—	37·6770	—	—	—	—
$^{176}Hf/^{177}Hf$	—	—	—	—	—	—	—
εHf	—	—	—	—	—	—	—

Table 3: continued

	Orhon		Gobi Altai		
Sample no.:	MN-30.5.1	MN-30.5.2	TB95-4.1	TB95-12.2	TB95-12.7.2
Latitude (N):	48°34·52′	48°34·52′	44°39·94′	43°30·65′	43°30·21′
Longitude (E):	103°08·42′	103°08·42′	102°12·99′	102°10·63′	102°09·92′
Lithology:	BTA	BTA	BTA	BTA	BTA
SiO_2	49·91	52·59	52·39	51·23	52·20
Al_2O_3	14·21	15·55	15·06	14·53	14·25
Fe_2O_3	10·65	10·12	9·55	10·19	9·91
MgO	6·61	5·53	4·16	6·54	6·33
K_2O	3·78	2·34	3·57	2·96	3·15
Na_2O	3·88	4·07	5·28	3·99	3·96
CaO	7·42	7·04	7·18	7·10	6·91
TiO_2	2·94	2·13	2·00	2·35	2·29
MnO	0·13	0·12	0·11	0·13	0·12
P_2O_5	1·01	0·57	0·76	0·78	0·71
Total	100·55	100·06	100·05	99·82	99·83
LOI	0·23	−0·45	2·8	1·42	1·83
Mg-no.	58·26	55·13	49·48	59·07	58·95
Rb*	48	38	29	47	61
Ba*	781	768	720	623	588
Th†	2·63	2·89	2·22‡	2·60‡	2·64‡
U†	0·45	0·69	—	—	—
Nb*	57·8	71·3	44·0	55·3	52·3
Ta	2·84	—	—	—	—
La†	35·27	35·09	29·90‡	30·30‡	29·80‡
Ce†	76·31	72·99	67·10‡	63·80‡	63·10‡
Pb†	2·70	3·65	1*	3*	4*
Pr†	10·41	9·64	—	—	—
Sr*	1065	1136	987	917	894
Nd†	43·85	40·74	40·02‡	36·13‡	35·85‡
Sm†	9·17	8·18	7·89‡	7·60‡	7·46‡
Zr*	237	221	227	217	214
Hf	—	5·30	5·51	5·01	5·00
Eu†	2·91	2·62	2·49‡	2·47‡	2·43‡
Gd†	7·64	7·01	5·17‡	5·73‡	5·22‡
Tb†	0·96	0·92	0·66‡	0·73‡	0·73‡
Dy†	4·62	4·54	—	—	—
Y*	21	20	18	20	19
Ho†	0·69	0·71	—	—	—
Er†	1·60	1·63	—	—	—
Tm†	0·18	0·20	—	—	—
Yb†	1·03	1·19	0·98‡	1·13‡	1·19‡
Lu†	0·14	0·16	0·12‡	0·15‡	0·15‡
Ni*	117	131	76	92	96
Cr*	167	146	114	113	103
ne	6·1	0·0	9·5	1·9	0·8
di	16·8	11·7	20·1	14·3	14·9
q	0·0	0·0	0·0	0·0	0·0
ol	12·5	8·7	7·0	13·6	12·8
hy	0·0	5·8	0·0	0·0	0·0
$^{87}Sr/^{86}Sr$	0·704363	—	—	0·704421¶	0·704491¶
$^{143}Nd/^{144}Nd$	0·512431	—	—	0·512313¶	0·512292¶
εNd	−4·04	—	—	−5·74	−6·75
$^{206}Pb/^{204}Pb$	17·7140	—	—	17·9110¶	18·0410¶
$^{207}Pb/^{204}Pb$	15·4500	—	—	15·4690¶	15·4850¶
$^{208}Pb/^{204}Pb$	37·6150	—	—	37·7890¶	37·9050¶
$^{176}Hf/^{177}Hf$	—	—	—	0·282769¶	—
εHf	—	—	—	0·65	—

Lithological abbreviations are the same as for Table 1. All major elements analysed by XRF (Leicester).
*Analysed by XRF (Leicester).
†Analysed by ICP-MS (Cardiff).
‡Analysed by INAA (Leicester); also Ta and Hf.
§Analysed by ICP-MS (Silwood Park).
¶Age-corrected data. [Uncorrected values for TB95-12.2: $^{87}Sr/^{86}Sr$ = 0·704492 (normalized); $^{143}Nd/^{144}Nd$ = 0·512344 (normalized); $^{206}Pb/^{204}Pb$ = 17·884; $^{207}Pb/^{204}Pb$ = 15·4299; $^{208}Pb/^{204}Pb$ = 37·6618; $^{176}Hf/^{177}Hf$ = 0·282772 (normalized). Uncorrected values for TB95-12.7.2: $^{87}Sr/^{86}Sr$ = 0·704584 (normalized); $^{143}Nd/^{144}Nd$ = 0·512265 (normalized); $^{206}Pb/^{204}Pb$ = 18·0135; $^{207}Pb/^{204}Pb$ = 15·4460; $^{208}Pb/^{204}Pb$ = 37·7768. Corrections to Pb were obtained by spiked isotope analysis.]

samples were crushed in a tungsten carbide mill to avoid Pb contamination from an agate mill, except for four crustal xenoliths (TB95-2.5, -10.3.4, -10.3.8a, -10.3.11c) that were crushed in an agate pestle. Whole-rock samples from the Gobi Altai were leached in hot 6M HCl for ~1 h to remove secondary alteration phases; whole-rock samples from Hangai are unaltered and therefore did not require acid leaching. Blanks for Sr, Nd and Pb were typically less than 125 pg, 275 pg, and 325 pg, respectively. $^{87}Sr/^{86}Sr$ was normalized during run time to $^{86}Sr/^{88}Sr = 0{\cdot}1194$; $^{143}Nd/^{144}Nd$ was normalized to a value of $^{146}Nd/^{144}Nd = 0{\cdot}7219$. Minimum uncertainties are derived from the external precision of standard measurements, which are 23 ppm (1σ) for $^{143}Nd/^{144}Nd$ and 21 ppm (1σ) for $^{87}Sr/^{86}Sr$. Sample data are reported relative to accepted values of NBS 987 of 0·71024 and 0·51186 for La Jolla.

Throughout the course of analysis, the Hf standard, JMC 475, yielded an average $^{176}Hf/^{177}Hf$ value of $0{\cdot}282170 \pm 9$ (1σ); sample data are reported relative to an accepted value of 0·282160. On the basis of repeated runs of NBS 981, the reproducibility of Pb-isotope ratios is better than $\pm 0{\cdot}1\%$. Pb isotope ratios were corrected relative to the average standard Pb isotopic compositions of Todt *et al.* (1993). Further details of analytical techniques have been given by Kempton (1995), Royse *et al.* (1998) and Nowell *et al.* (1998*a*). Data are reported in Table 3.

Argon dating

Little information exists on the timing of volcanism in Mongolia, particularly for the Gobi Altai. From compilations of available age data (e.g. Whitford-Stark, 1987), there appear to be two episodes of volcanism within the Hangai region, one Miocene ($<12 \pm 1$ Ma) and the other Quaternary. The age relationship of volcanism in the Gobi Altai to that in Hangai is essentially unknown. Consequently, whole-rock $^{40}Ar/^{39}Ar$ dating, using the incremental heating technique, was undertaken to establish whether the timing of volcanism in the Gobi Altai is similar to that in Hangai. Three samples were chosen from the Gobi Altai (TB95-2.10, -12.2, -12.7.2) and two from Hangai (MN-10.1.1 and -11.2.2; Table 2). Sample selection was based on geographical locality, high total alkali ($K_2O + Na_2O$) content, freshness of feldspars, and minimal content of glass (to reduce the risk of including highly altered, fine-grained material). The samples were prepared by taking cores of 6 mm diameter from a fresh sample, with slices of 1 mm thickness taken from the cores. The slices were then sealed in a quartz vial along with sanidine neutron flux monitor standards and the samples were irradiated at the Oregon State University Triga reactor in a cadmium-shielded CLILIT facility. Neutron flux monitor, J, was measured, and is quoted for each experiment (supplementary data may be downloaded from the *Journal of Petrology* website at http://www.petrology.oupjournals.org). The samples were analysed at the SUERC/NSS Ar facility, East Kilbride.

ARGON DATING RESULTS

Results are summarized in Table 2, and the full dataset is available for downloading from the *Journal of Petrology* website at http://www.petrology.oupjournals.org. Weighted plateau ages were calculated, with each step age weighted by the inverse of its variance (Fig. 2; Table 2), therefore ensuring that poor quality data do not have a disproportionate effect on the age result. Age spectra and isochron ages ($^{40}Ar/^{36}Ar$ vs $^{39}Ar/^{36}Ar$) were also calculated for all incremental heating experiments (Table 2). All errors are quoted at one standard deviation.

All samples produced an arguably meaningful age; either a date has an MSWD (mean square weighted deviation) value close to unity, or the $^{40}Ar/^{36}Ar$ intercept is within error of 295·5 (value for atmospheric $^{40}Ar/^{36}Ar$), or there is close agreement between the weighted age and the isochron age. The Ar–Ar ages show that the volcanism in the Gobi Altai (~33 Ma) is significantly older than that in Hangai (<6 Ma). The Oligocene volcanism of the Gobi Altai is also the oldest well-constrained Cenozoic magmatism currently documented for Mongolia. Whether volcanism was continuous from the Oligocene or whether it was restricted to discrete time intervals is unknown from the limited data available.

GEOCHEMISTRY OF CENOZOIC MONGOLIAN BASALTS

Major elements and compatible trace elements

Volcanic rocks from Hangai range in composition from transitional alkali basalts, trachybasalts to tephrite basanites and their differentiates (Fig. 3a). Most samples are nepheline (ne)-normative, but hypersthene (hy)-normative compositions also occur (Fig. 3b). The older lavas from the eastern Gobi Altai tend to be more evolved, being predominantly basaltic trachyandesites and trachyandesites (Fig. 3a) that are weakly to moderately ne-normative (Table 3). The majority of the lavas from Hangai have low LOI values below 1 wt %, consistent with the overall freshness of the lavas. In contrast, lavas from the Gobi Altai show petrographic evidence of alteration in the presence of iddingsite and sericite (Table 1), and have higher LOIs that range from 0·7 to 2·8 wt %.

Variations of selected major elements and incompatible trace elements relative to Mg-number [100Mg/(Mg +

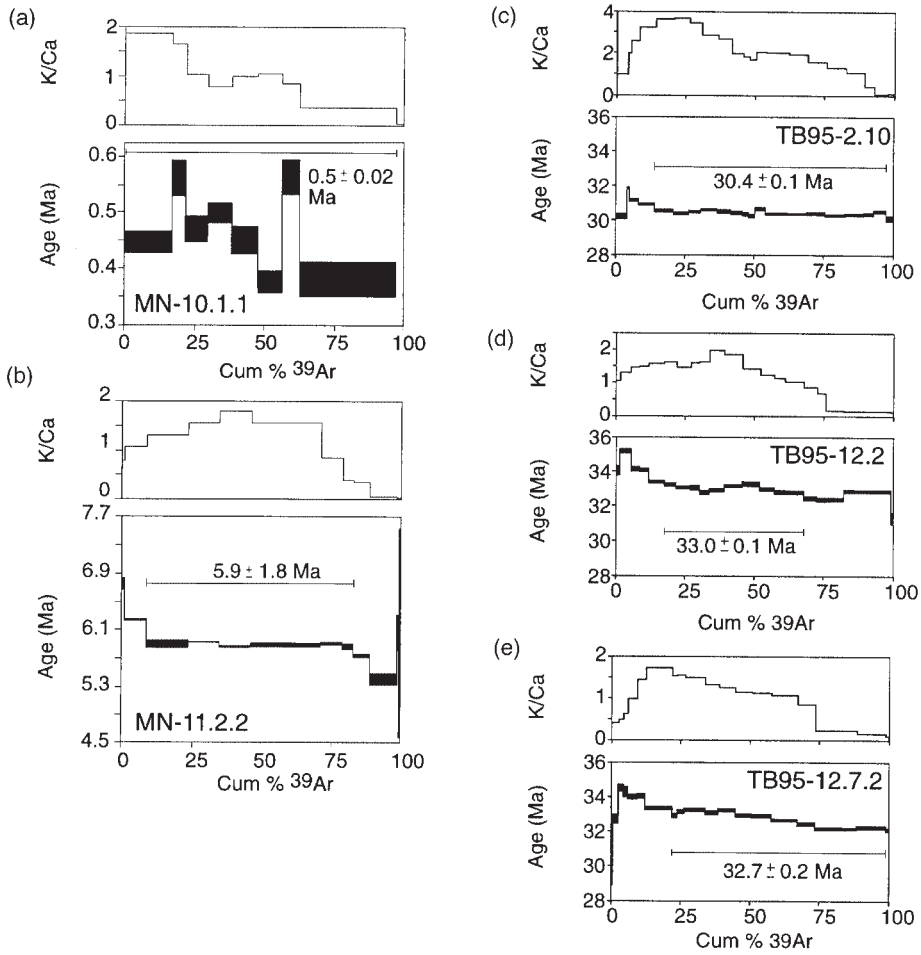

Fig. 2. Ar–Ar age plateau diagrams for Tariat volcanic province and the Gobi Altai. Tariat samples: (a) MN-10.1.1 from the Chuloot Formation; (b) MN-11.2.2 from the Morun Formation. Gobi Altai samples: (c) TB95-2.10 from the Bogd Plateau; (d) TB95-12.2 and (e) TB95-12.7.2 from the Sevrei Plateau.

Fe)] are shown in Fig. 4. SiO_2 and Fe_2O_3 define curvilinear trends when plotted against Mg-number (Fig. 4), with rocks from the eastern Gobi Altai being the most evolved, i.e. Mg-number as low as 31. Three basalts from Togo (MN-27.1, -27.3.1 and -28.4) have moderately high Mg-numbers (~67), as well as high Ni contents (~300), suggesting that they may have accumulated olivine phenocrysts or contain disaggregated mantle xenocrysts (Table 1); these same lavas also have high Cr contents (~390), which implies accumulation of Cr spinel.

Na_2O, K_2O, CaO, P_2O_5, Al_2O_3 and TiO_2 show considerable scatter when plotted against Mg-number, particularly for the Hangai data. A sub-linear correlation is observed for CaO/Al_2O_3, suggesting that clinopyroxene is an important phase in the differentiation of the magmas.

Tariat volcanic rocks tend to have low TiO_2 compared with other lavas from Hangai, but span the complete range of CaO/Al_2O_3 values of all the other Hangai lavas (Fig. 4). In studies of continental flood basalt provinces, distinct basalt groups with low and high Ti have frequently been identified [e.g. Paraná (Gibson *et al.*, 1995) and Ethiopia (Pik *et al.*, 1998, 1999)]; these have commonly been interpreted as evidence for the involvement of lithospheric and asthenospheric mantle source components in the petrogenesis of the magmas, respectively. In some cases (e.g. Paraná; Peate & Hawkesworth, 1996) the high- and low-Ti groups appear to be temporally controlled, with low-Ti basalts inferred to reflect early melts of a hydrated but relatively refractory lithospheric mantle source whereas later phases of magmatism (high-Ti) are the products of partial melting of relatively fertile asthenosphere. However, no such temporal change in Ti contents is evident for the Mongolian basalts. The situation in Mongolia may be more similar to that in Ethiopia (Pik *et al.*, 1998, 1999), where a geographical control is observed. In Mongolia the low-Ti group is almost exclusively restricted to lavas from Tariat, whereas the high-Ti lavas occur in the remaining localities of Hangai.

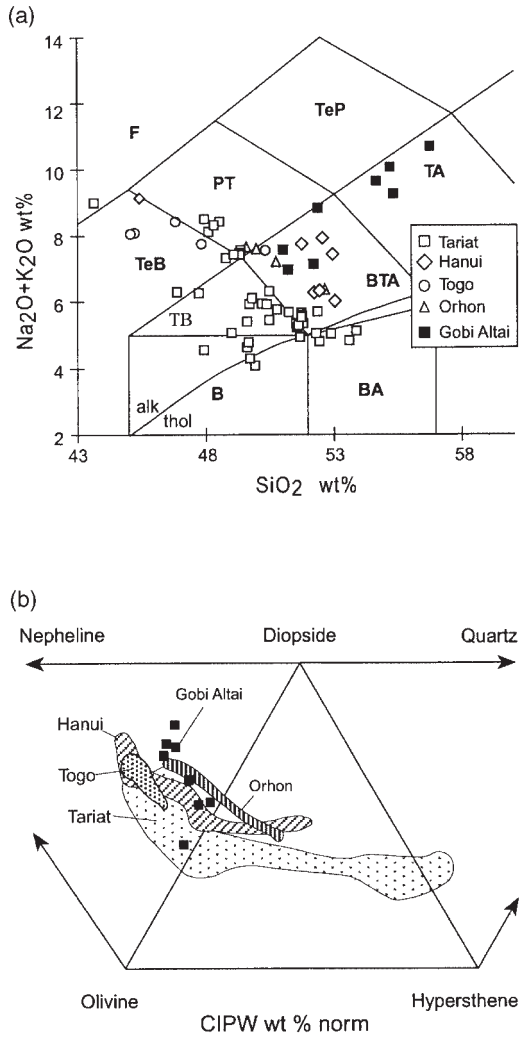

Fig. 3. (a) Total alkalis ($Na_2O + K_2O$) vs SiO_2 (from Le Bas *et al.*, 1986) for all analysed Mongolian Cenozoic basalts. B, basalt; BA, basaltic andesite; TB, trachybasalt (hawaiite); BTA, basaltic trachyandesite (mugearite); TA, trachyandesite (benmoreite); PT, phonotephrite; TeB, tephrite basanite; F, foidite; TeP, tephri-phonolite. (b) CIPW-norm (di–hy–ol–ne–qz) diagram plotted using Fe_2O_3/FeO = 0·2 for all Mongolian Cenozoic basalts. Trend of the Tariat field suggests high-pressure fractionation (Thompson, 1974). It should be noted that the Hangai data have been plotted as fields to simplify the diagram. ■, data from the Gobi Altai.

The Gobi Altai basalts have intermediate TiO_2 contents between Tariat and the other Hangai lavas.

Incompatible trace elements

Trace element data are plotted on primitive mantle-normalized variation diagrams in Fig. 5. Shown for comparison are the compositions of average OIB (Sun & McDonough, 1989) and high-Ti and low-Ti basalts from Paraná (Gibson *et al.*, 1995) and Ethiopia (Pik *et al.*, 1998, 1999). Clear differences exist between the Mongolian basalts and the high- and low-Ti basalts of Ethiopia, with only a moderate degree of similarity to the low-Ti basalts of Paraná (Fig. 5e and f). The diagrams show that all Mongolian volcanic rocks are enriched in large ion lithophile elements (LILE) and light rare earth elements (LREE) relative to heavy rare earth elements (HREE). All the trace element patterns show moderately high Nb, K, P and Sr, and most have negative Pb anomalies (Fig. 5). The Mongolian basalts are depleted in Th and U relative to K, and most have K_n/Nb_n ratios >1. Nb concentrations are relatively high and are highest in lavas from Togo (Nb 87–121 ppm), with positive Nb relative to adjacent elements U (and Th) and K (Fig. 5c).

All of the samples, regardless of age or location, show similar chondrite-normalized REE patterns (Fig. 6). However, the Hanui volcanic rocks are slightly less LREE enriched (La_n/Yb_n = 11·18–20·21) than other Hangai samples (La_n/Yb_n = 13·14–46·57). In this regard the rocks from Hanui are more similar to the volcanic rocks of the Gobi Altai (La_n/Yb_n = 17·96–19·33).

Isotope variation

Strontium, neodymium and lead isotopes

Fifteen samples from each of the geographical localities and encompassing the full range of chemical diversity were selected for Sr, Nd and Pb isotope analysis. The data are presented in Table 3.

$^{143}Nd/^{144}Nd$ and $^{87}Sr/^{86}Sr$ data are plotted in Fig. 7, together with published data for other Tertiary basalts from NE China (Song *et al.*, 1990; Basu *et al.*, 1991; Tatsumoto *et al.*, 1992; Han *et al.*, 1999) as well as fields for mantle xenoliths from Tertiary basalts in Mongolia (Stosch *et al.*, 1986; Ionov *et al.*, 1994; Wiechert *et al.*, 1997), the Lake Baikal region of Russia (Ionov *et al.*, 1992, 1995) and NE China (Tatsumoto *et al.*, 1992). The Tertiary basalts from China and the mantle xenoliths from Mongolia, Russia and China are plotted for comparison because of their similar tectono-magmatic settings to that of the Mongolian lavas.

The Mongolian basalts plot close to bulk silicate Earth (BSE) (Fig. 7), overlapping with previously published data for Cenozoic basalts from China (Song *et al.*, 1990; Basu *et al.*, 1991; Tatsumoto *et al.*, 1992). Some samples (e.g. from Togo, Orhon and the Gobi Altai), however, have significantly lower Nd isotope compositions, down to 0·512292 (Fig. 7). However, none of the samples overlap with the field for Pacific MORB (P-MORB), plotted as representative of depleted mantle proximal to Asia, but do overlap with the enriched extreme of Indian-MORB (I-MORB), also a possible contributor to the

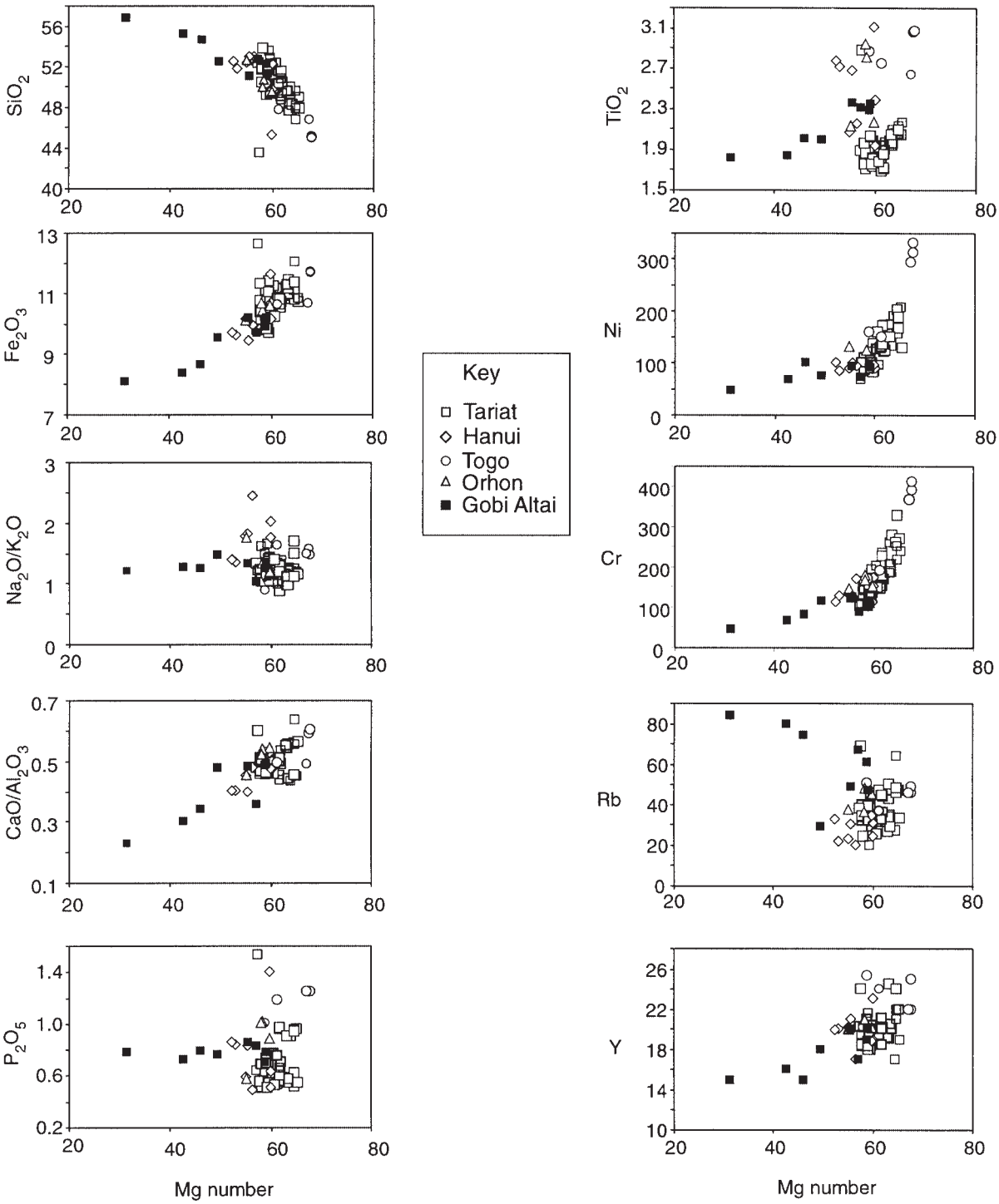

Fig. 4. Variation diagrams of Mg-number vs SiO_2, $Fe_2O_{3(tot)}$, Na_2O/K_2O, CaO/Al_2O_3, P_2O_5, TiO_2, Ni, Cr, Rb and Y for Hangai and Gobi Altai rocks.

Asian shallow mantle. The Mongolian basalts are generally less depleted than Mongolian mantle xenoliths (Stosch *et al.*, 1986; Ionov *et al.*, 1994; Wiechert *et al.*, 1997).

On a plot of $^{207}Pb/^{204}Pb$ vs $^{206}Pb/^{204}Pb$ (Fig. 8a) the Mongolian basalts define a trend sub-parallel to the Northern Hemisphere Reference Line (NHRL), and lie within the field for I-MORB, slightly overlapping P-

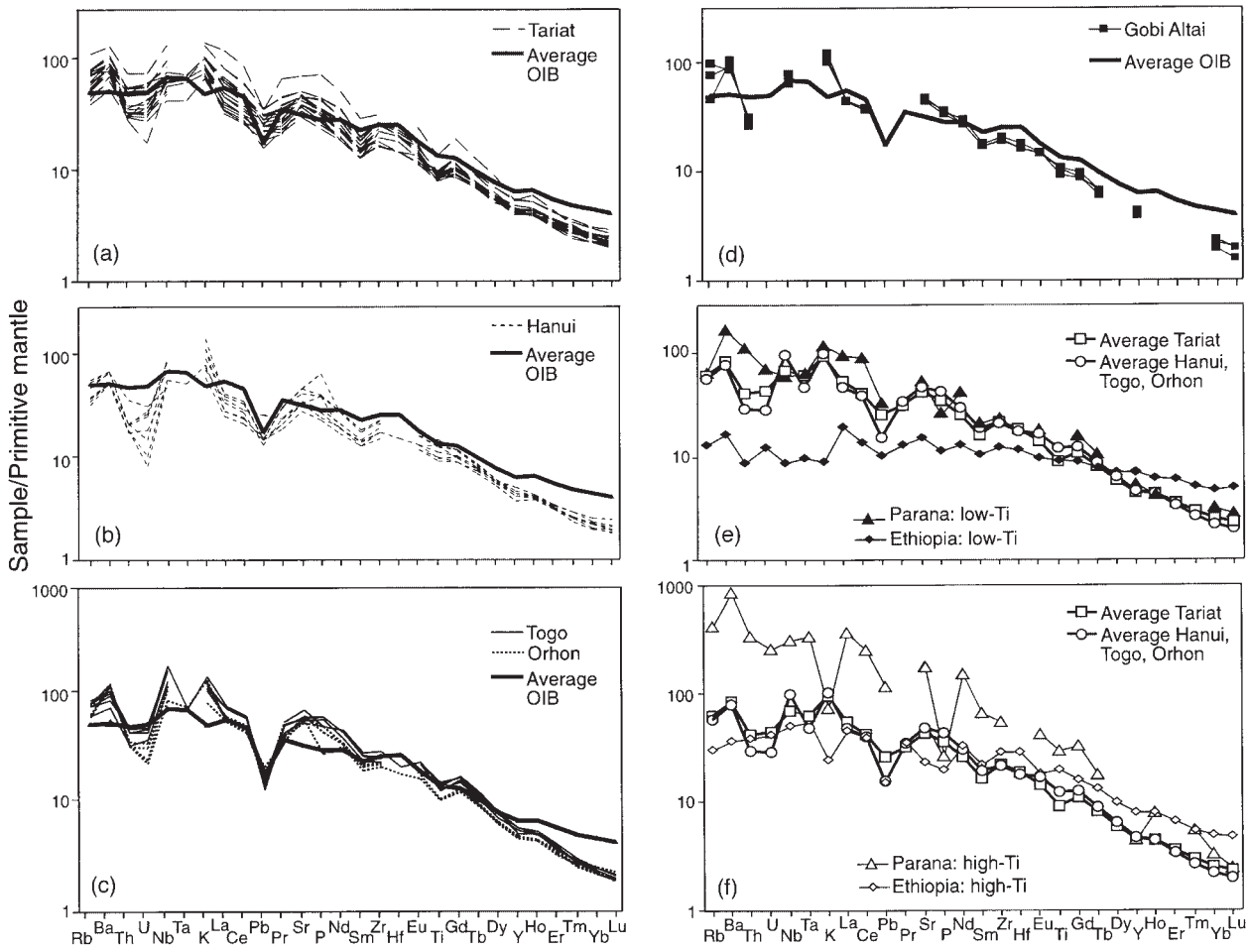

Fig. 5. Mantle-normalized trace element variation diagrams for: (a) Tariat volcanic province; (b) Hanui volcanic province; (c) Togo and Orhon volcanic provinces; (d) the Gobi Altai volcanic rocks (although some elemental data not available); (e) and (f) low-Ti and high-Ti volcanic provinces, respectively, with average data for the Mongolian volcanic provinces for comparison. Data sources: Parana: Gibson *et al.* (1995); Ethiopia: Pik *et al.* (1998, 1999); average OIB: Sun & McDonough (1989); normalization values for primitive mantle: Sun & McDonough (1989).

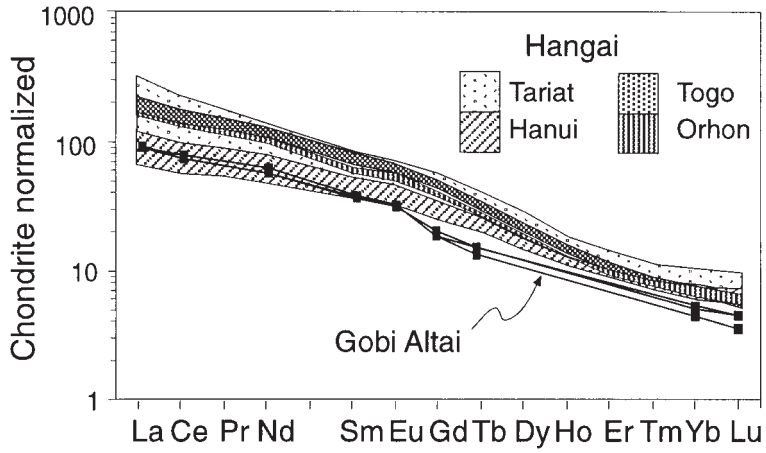

Fig. 6. Chondrite-normalized REE plots for Tariat, Hanui, Togo, Orhon and Gobi Altai volcanic provinces. Normalization values from Sun & McDonough (1989).

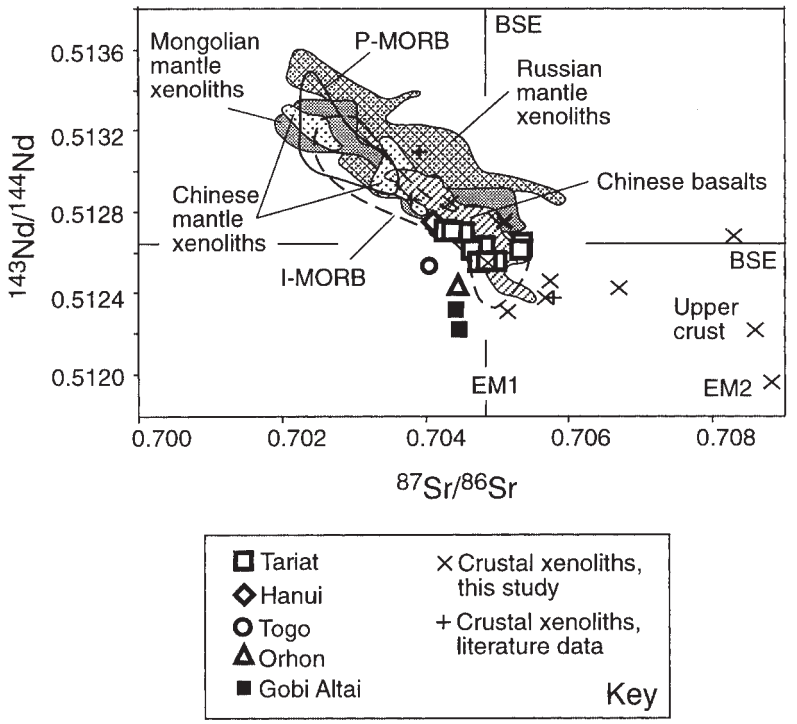

Fig. 7. Variation of $^{143}Nd/^{144}Nd$ vs $^{87}Sr/^{86}Sr$ for all Mongolian basalt data (analytical error less than the size of the symbols). Older Gobi Altai samples are age corrected. Data sources: Chinese basalts: Song *et al.* (1990), Basu *et al.* (1991) and Tatsumoto *et al.* (1992); Chinese mantle xenoliths: Tatsumoto *et al.* (1992); Mongolian mantle xenoliths (Dariganga and Tariat): Stosch *et al.* (1986), Ionov *et al.* (1994) and Wiechert *et al.* (1997); Russian mantle xenoliths: Ionov *et al.* (1992, 1995); crustal xenoliths: Stosch *et al.* (1995); I-MORB: Cohen & O'Nions (1982), Hamelin & Allègre (1985), Hamelin *et al.* (1986), Michard *et al.* (1986), Ito *et al.* (1987), Dosso *et al.* (1988), Klein *et al.* (1988), Mahoney *et al.* (1989, 1992) and Pyle *et al.* (1992); P-MORB: Cohen & O'Nions (1982), White & Hofmann (1982), MacDougall & Lugmair (1986), Ito *et al.* (1987), White *et al.* (1987), Klein *et al.* (1988), Pyle *et al.* (1992), Ferguson & Klein (1993), Bach *et al.* (1994), Mahoney *et al.* (1994), Niu *et al.* (1996), Schiano *et al.* (1997), Castillo *et al.* (1998) and Vlastélic *et al.* (1999); EM1 and EM2: Zindler & Hart (1986); BSE: Zindler & Hart (1986).

MORB. The higher $^{206}Pb/^{204}Pb$ Hangai lavas plot near the NHRL but most samples trend toward lower $^{206}Pb/^{204}Pb$ values similar to some anomalous MORBs on the Southwest Indian Ridge (Mahoney *et al.*, 1996) and typical of an EM1-type mantle component. The $^{208}Pb/^{204}Pb$ values of the Mongolian lavas are, however, lower than most EM1-type compositions (Fig. 8b), but still follow the trend of low $^{206}Pb/^{204}Pb$ I-MORB samples.

Hafnium isotopes

Six samples from Tariat were selected for a study of Hf isotopes, to examine temporal changes in source characteristics and the relative contributions from either a garnet- or spinel-facies source. The study was restricted to Tariat only, because the province provides good relative age constraints, whereas the timing of volcanism in the other provinces is much more uncertain. Samples with high MgO, Ni and Cr, and low Sr and Zr contents were selected, to represent the least likely crustally contaminated magmas and therefore the most primary mantle-derived magmas. $^{176}Hf/^{177}Hf$ isotope ratios range from 0·282713 to 0·282992 (Table 3), and lie within the field of ocean island basalts on a plot of εHf vs εNd (Fig. 9). This indicates that the source of the Mongolian volcanic rocks has lower time-integrated Lu/Hf and Sm/Nd than most mid-ocean ridge basalts derived from the asthenosphere. Two samples plot above the mantle array (MN-5.2.2 and MN-11.2.2), indicating a slightly higher time-integrated Lu/Hf in their source compared with the other Tariat samples. However, it should be noted that the Mongolian basalt data form a trend with a steeper slope than that of the mantle array and could be inferred to trend toward the composition of lamproites derived from ancient lithospheric mantle (Nowell *et al.*, 1999). In this regard, it is interesting to note that the Mongolian basalts also overlap with the compositions of late Cenozoic basaltic rocks from NW Colorado and the Rio Grande Rift, USA (Beard & Johnson, 1993; Johnson & Beard, 1993), which have been interpreted as having a lithospheric mantle source.

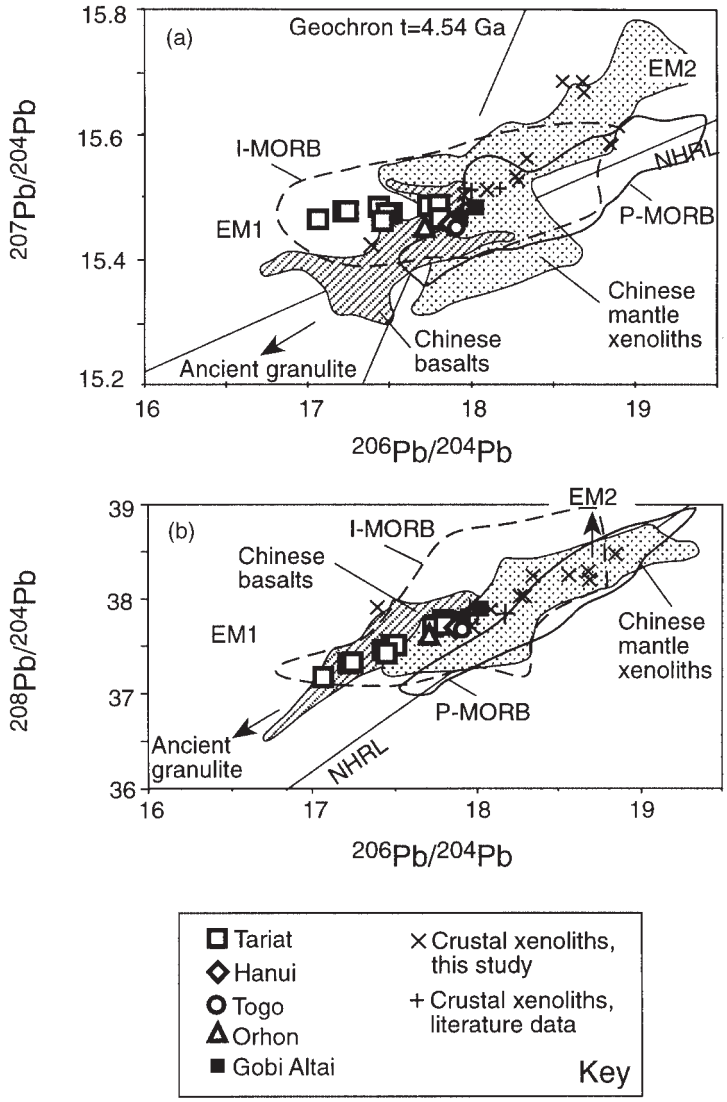

Fig. 8. (a) Variation of $^{207}Pb/^{204}Pb$ vs $^{206}Pb/^{204}Pb$ for all Mongolian basalt data (analytical error less than the size of the symbols). Data sources: Chinese basalts and Chinese mantle xenoliths: same as in Fig. 7; I-MORB: same as in Fig. 7 with additional data from Price *et al.* (1986); P-MORB: same as in Fig. 7, excepting White & Hofmann (1982) and MacDougall & Lugmair (1986), but additional data from Dupré *et al.* (1981), Hamelin *et al.* (1984) and Hanan & Schilling (1989); NHRL: Hart (1984); ancient granulite: Taylor & McClennan (1985); EM1 and EM2: Zindler & Hart (1986). (b) A plot of $^{208}Pb/^{204}Pb$ vs $^{206}Pb/^{204}Pb$ for all Mongolian basalt data. Data sources: same as for (a).

GEOCHEMISTRY OF THE MONGOLIAN CRUST; XENOLITH DATA

Before this study, evaluating the role of crustal contamination in the petrogenesis of the Mongolian lavas had been complicated by the lack of chemical and isotopic data for the composition of the continental crust of central Mongolia. Existing data suggest that the crust is ~45 km thick (Kopylova *et al.*, 1995) and consists of an amalgamation of Precambrian to Palaeozoic micro-continental blocks, arc terranes and orogenic fold belts (Cunningham, 2001). Therefore, it is likely to be highly diverse and variable in age.

Previously studied crustal xenoliths from Tariat are predominantly LREE-enriched two-pyroxene lower-crustal granulites (e.g. La_n/Yb_n = 0·9–14·3; Stosch *et al.*, 1995), although mid-crustal amphibolite-facies felsic lithologies are also observed. On the basis of the chemical composition of the granulite xenoliths, Stosch *et al.* (1995) concluded that their protoliths formed by basaltic underplating at the crust–mantle boundary. Unfortunately, Stosch *et al.* (1995) reported Sr, Nd and Pb isotope data for only one crustal xenolith from Tariat, sample 8531/

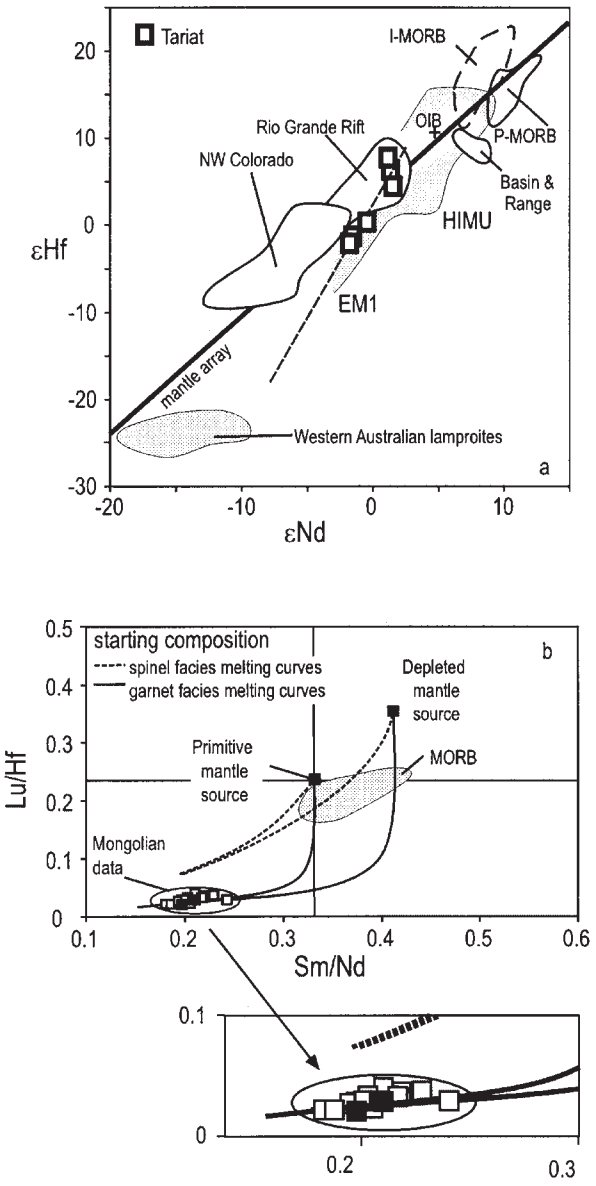

Fig. 9. (a) A plot of εHf vs εNd for Tariat samples. Dashed line shows that the Mongolian data have a steeper trend than the mantle array. Data sources: mantle array (bold black line): Vervoort & Blichert-Toft (1999); P-MORB and I-MORB: Nowell *et al.* (1998*a*), Chauvel & Blichert-Toft (2001) and Kempton *et al.* (2002); OIB: Nowell *et al.* (1998*a*) and Chauvel & Blichert-Toft (2001); western Australian lamproite field: Nowell *et al.* (1999); NW Colorado, Basin and Range, and Rio Grande Rift: Beard & Johnson (1993) and Johnson & Beard (1993); EM1 and HIMU: Salters & Hart (1991). (All published data normalized to JMC-475 = 0·282160.) (b) Lu/Hf vs Sm/Nd melting models predicting melt compositions from primitive and depleted mantle sources with melting occurring in the spinel and garnet facies. Data sources: partition coefficients: Chauvel & Blichert-Toft (2001); MORB field: Chauvel & Blichert-Toft (2001); primitive mantle source: Sun & McDonough (1989); depleted mantle source calculated from the residue after extraction of 15% melt from a primitive mantle starting composition. Melting curves calculated using the fractional melting equations of Albarède (1995).

46 ($^{87}Sr/^{86}Sr$ = 0·705755, $^{143}Nd/^{144}Nd$ = 0·512375, $^{206}Pb/^{204}Pb$ = 17·962), although Nd isotope data are available for two other samples ($^{143}Nd/^{144}Nd$ = 0·512513 and 0·512579). Additionally, Stosch *et al.* (1995) reported isotope data for two crustal xenoliths from Dariganga, but Dariganga is located ~800 km away from Tariat and the Gobi Altai, and these two xenoliths have considerably higher $^{143}Nd/^{144}Nd$ ratios (0·512854 and 0·513086) than that of the Tariat xenoliths.

Therefore, for the purpose of assessing the role of continental crust in the petrogenesis of the Mongolian lavas, this study presents new geochemical data for crustal xenoliths from Mongolia (Table 4). Four crustal xenoliths from the Gobi Altai were collected: TB95-2.5, a course-grained granulite, from the Bogd Plateau (Fig. 1d); TB95-10.3.4 and -10.3.11c, both two-pyroxene granulites; and TB95-10.3.8a, an unusual feldspar–quartz-rich rock that has undergone a partial melting or melt extraction event, from a Mesozoic volcanic plug situated between the Bogd and Sevrei Plateaux. A further seven crustal xenoliths described by Stosch *et al.* (1995) were analysed for their Sr, Nd and Pb isotopic compositions as well as major, trace and rare earth elements (Table 4).

DISCUSSION

Sr–Nd–Pb–Hf isotopic data presented in Figs 7–9 indicate that the Mongolian basalts have compositions that are distinct from MORB-source mantle. If the parental magmas were derived from the shallow asthenosphere, their original compositions must have been modified by interaction with crust or lithospheric mantle. Alternatively, the Mongolian parental magmas may have been derived from a plume source with subsequent contamination by crust or lithospheric mantle. Here we consider these various alternatives and begin by assessing the possible influence of shallow-level magma chamber processes (fractional crystallization and crustal contamination).

Shallow-level processes

Fractional crystallization

Much of the variation in the major element composition of the Mongolian volcanic rocks is likely to be a consequence of fractional crystallization. MgO contents (1·64–10·99 wt %) and Mg-numbers (31·3–67·8) for most lavas are too low to be in equilibrium with mantle olivine, indicating that these are not primary melts. On the basis of the phenocryst assemblages observed, olivine is the main liquidus phase in the basalts (Table 1), but clinopyroxene is the main phenocryst phase in samples MN-11.2, MN-11.2.1 and MN-11.2.2 from the Morun Formation, Tariat (Table 1). A broad trend of decreasing

Table 4: Geochemical data for crustal xenoliths from Mongolia

	Dariganga			Gobi Altai				Tariat					
Sample:	8505/67	8519/52	8523/14	TB95-2.5	TB95-10.3.4*	TB95-10.3.8a*	TB95-10.3.11c*	4399/16	4399/17	4399/20	8531/44	8531/45	8531/46
Lithology:	Granulite	Granulite	Granulite	Granulite	Granulite	Melt residue	Granulite	Granulite	Granulite	Granulite	Unspecified	Granulite	Granulite
SiO_2	53·40†	54·25†	53·45†	—	—	—	—	58·75†	53·20†	56·75†	65·75†	52·06†	50·90†
Al_2O_3	9·60†	17·40†	18·70†	14·14	16·91	—	—	15·60†	18·20†	17·20†	15·10†	18·20†	9·30†
Fe_2O_3	12·92†	9·13†	6·27†	8·90	10·38	—	—	8·70†	8·73†	5·82†	6·18†	9·25†	13·01†
MgO	14·50†	5·19†	6·51†	6·80	7·21	—	—	4·02†	4·07†	3·65†	1·85†	6·57†	12·70†
K_2O	0·12†	0·79†	0·72†	0·55	0·47	—	—	1·06†	1·07†	2·00†	1·92†	0·48†	0·75†
Na_2O	1·55†	4·35†	3·58†	2·39	3·68	—	—	4·60†	4·94†	5·06†	4·12†	3·90†	1·68†
CaO	8·77†	8·27†	10·40†	16·47	8·35	—	—	6·33†	8·06†	7·53†	4·04†	9·33†	11·30†
TiO_2	0·50†	1·01†	0·66†	1·85	0·56	—	—	0·88†	1·17†	1·16†	0·84†	0·98†	1·20†
MnO	0·23†	0·16†	0·14†	0·11	0·34	—	—	0·17†	0·14†	0·10†	0·18†	0·17†	0·23†
P_2O_5	0·09†	0·17†	0·08†	—	—	—	—	0·12†	0·39†	0·40†	0·29†	0·23†	0·40†
Total	102·0†	101·2†	100·9†	—	—	—	—	100·8†	100·3†	100·2†	101·3†	101·5†	101·9†
LOI	0·35†	0·45†	0·40†	—	—	—	—	0·55†	0·30†	0·55†	1·05†	0·35†	0·45†
Mg-no.	71·62†	56·10†	70·01†	63·21	60·96	—	—	50·96†	51·18†	58·51†	40·23†	61·49†	68·70†
Co	72	30	38	23	32	—	—	24	23	19	5	32	61
Ba	52	222	136	638	89	—	—	211	595	1285	823	115	369
Th	b.d.l.	b.d.l.	0·7	0·2	0·2	9·6	0·2	0·6	0·2	0·5	2·6	b.d.l.	b.d.l.
Ni	86	46	50	46	44	—	—	34	32	58	14	58	93
Cr	181	64	66	112	80	—	—	45	18	43	4	104	233
Zn	147	99	44	99	91	—	—	83	82	67	78	78	124
Nb	2·8	1·7	8·6	3·8	1·2	6·2	1·3	5·1	0·9	2·2	6·5	1·6	2·5
Cu	48	44	62	62	46	—	—	58	41	46	26	46	96
V	215	164	285	277	171	—	—	167	198	148	60	190	225
Rb	b.d.l.	1·2	5·1	4·3	5·8	83·2	4·9	3·9	3·1	7·2	26·2	0·7	16·9
Sr	157	596	546	604	588	—	—	293	1214	1403	385	572	470

Table 4: continued

	Dariganga			Gobi Altai				Tariat					
Sample:	8505/67	8519/52	8523/14	TB95-2.5	TB95-10.3.4*	TB95-10.3.8a*	TB95-10.3.11c*	4399/16	4399/17	4399/20	8531/44	8531/45	8531/46
Lithology:	Granulite	Granulite	Granulite	Granulite	Granulite	Melt residue	Granulite	Granulite	Granulite	Granulite	Unspecified	Granulite	Granulite
Pb	0·1	3·5	63·3	0·7	1·2	26·0	4·9	44·7	4·7	7·2	7·4	14·4	1·6
Be	0	1	1	1	1	—	—	1	1	1	1	1	1
Zr	73·2	44·9	45·4	70·8	16·0	91·7	21·2	69·0	21·2	73·1	145·6	41·0	44·0
Hf	1·9	0·7	0·6	2·0	0·4	1·8	0·2	2·0	0·2	1·7	3·0	0·4	1·1
Sc	45†	25†	25†	—	—	—	—	24†	18†	13†	20†	25†	48†
Y	26·5	10·6	7·0	12·8	10·2	26·6	12·8	15·5	8·2	7·5	16·3	8·2	21·5
La	3·6	5·8	6·6	17·9	2·5	18·5	3·9	10·1	13·7	14·2	12·0	6·8	15·3
Ce	11·8	15·5	13·9	49·4	6·9	36·2	9·1	21·2	29·1	30·3	27·7	15·2	40·6
Pr	2·3	2·4	1·8	8·0	1·2	3·8	1·5	2·8	4·0	4·4	3·5	2·2	6·1
Nd	13·1	11·6	8·3	38·1	5·8	13·5	7·3	11·3	17·9	19·3	14·8	9·8	27·5
Sm	4·2	2·7	2·2	8·0	1·9	2·3	2·4	2·7	3·5	4·3	3·0	2·2	6·4
Eu	0·8	1·0	1·5	1·9	0·9	0·6	1·0	1·0	1·4	1·3	1·2	1·0	1·2
Gd	4·6	2·6	2·2	6·4	2·1	2·9	2·5	3·1	3·3	3·5	3·2	2·2	6·0
Tb	0·8	0·4	0·3	0·8	0·3	0·5	0·4	0·4	0·4	0·4	0·5	0·3	0·9
Dy	4·9	2·4	1·8	3·7	2·2	3·6	2·6	2·8	2·0	2·0	3·4	1·9	4·3
Ho	1·0	0·5	0·4	0·6	0·5	0·9	0·6	0·6	0·4	0·4	0·7	0·4	1·0
Er	2·8	1·2	0·9	1·4	1·3	3·0	1·6	1·9	1·0	0·9	2·0	1·0	2·4
Tm	0·4	0·2	0·1	0·2	0·2	0·5	0·2	0·3	0·2	0·1	0·3	0·2	0·4
Yb	2·8	1·3	0·8	0·8	1·3	3·5	1·7	1·9	0·9	0·8	2·3	1·0	2·3
Lu	0·4	0·2	0·1	0·1	0·2	0·5	0·3	0·3	0·1	0·1	0·4	0·1	0·4
$^{87}Sr/^{86}Sr$	—	—	0·704363	0·708585	0·705106	0·708289	0·705104	0·706702	0·704873	0·705732	0·708817	0·705150	0·705706
$^{143}Nd/^{144}Nd$	—	—	0·512843	0·512221	0·512740	0·512679	0·512751	0·512420	0·512546	0·512457	0·511965	0·512305	0·512373
$^{206}Pb/^{204}Pb$	—	—	18·688	18·342	18·274	18·845	18·292	18·679	17·969	18·096	17·394	18·561	17·955
$^{207}Pb/^{204}Pb$	—	—	15·669	15·562	15·533	15·587	15·527	15·685	15·491	15·512	15·425	15·685	15·504
$^{208}Pb/^{204}Pb$	—	—	38·208	38·248	38·033	38·484	38·028	38·291	37·715	37·878	37·916	38·250	37·871

Sample 8531/44, labelled 'unspecified' lithology, is of lower metamorphic, amphibolite-facies grade and consists of plagioclase, mica, epidote and quartz (Stosch *et al.*, 1995). Xenoliths erupted in Cenozoic basalts except three Mesozoic samples (marked *). †Samples reported by Stosch *et al.* (1995). Elements Th, Nb, Rb, Pb, Zr, Hf, Y, La, Ce, Pr, Nd, Sm, Eu, Gd, Tb, Dy, Ho, Er, Tm, Yb and Lu analysed by ICP-MS at the NERC facility, Silwood Park, Ascot. All other elemental data by ICP-AES at the University of Leicester. Isotopic data from NIGL, all normalized values. b.d.l., below detection limit.

CaO/Al_2O_3 vs Mg-number confirms the role of clinopyroxene in controlling magmatic differentiation and indicates that fractionation of feldspar was probably insignificant (Fig. 4). Barry (1999) demonstrated that low-pressure ($< \sim 12$ kbar) fractional crystallization of a single parental magma could not account for the range of compositional variations observed. Instead, each volcanic province appears to require a different parental magma to account for the various liquid lines of descent, and therefore they are not cogenetic.

Some of the scatter in the data may be due to fractionation at higher pressures, which may involve garnet in sub-crustal magma bodies. Samples from the Gobi Altai show a positive correlation between Mg-number and HREE, Y and Sc (e.g. Mg-number vs Y, Fig. 4). This is consistent with high-pressure fractionation involving garnet, olivine and perhaps clinopyroxene. However, none of the other suites show this effect and therefore we conclude that, with the exception of the Gobi Altai samples, high-pressure fractionation may be limited, and we must resort to other processes to account for the compositional variations.

Crustal contamination and AFC

Bulk assimilation of wallrock is commonly invoked for open-system magma chamber processes. This process can be tested using a simple plot of 1/Sr vs $^{87}Sr/^{86}Sr$ (Fig. 10a), because any mixing between a parental basalt composition and crustal material should plot as a straight line, assuming no fractional crystallization. Figure 10a illustrates mixing lines for possible contamination trends between parental magmas represented by MN-25.1 and MN-27.4 (samples with the highest $^{143}Nd/^{144}Nd$ and lowest $^{87}Sr/^{86}Sr$ values) and two end-member composition crustal xenoliths from Tariat (8531/44, mid-crust, and 4399/16, lower crust; this paper). This suggests that there has been no mixing with continental crust. It should be noted that most of the crustal xenoliths have lower Sr contents than the lavas. It would be difficult, although not impossible (e.g. Bohrson & Spera, 2001), to assimilate such material and have a significant impact on the $^{87}Sr/^{86}Sr$ ratios of the lavas while simultaneously maintaining their relatively high Mg-numbers. The conclusion that bulk assimilation has not played a significant role in magma genesis is further emphasized in plots of $^{143}Nd/^{144}Nd$ vs Nd (Fig. 10b) and $^{143}Nd/^{144}Nd$ vs $^{206}Pb/^{204}Pb$ (Fig. 10c). Both of these plots show that the majority of Mongolian samples form arrays that are distinctly different from the fields for lower-crustal xenoliths, i.e. the Mongolian lavas do not trend toward crust as would be expected for bulk assimilation. The volcanic rocks not only have generally higher $^{143}Nd/^{144}Nd$ than the majority of crustal xenoliths but also higher Nd concentrations (Fig. 10b). Following the same logic as applied to the Sr data, this means that bulk assimilation of lower continental crust cannot account for the compositional variations observed. Figure 10c shows that most of the volcanic rocks form an array, which if extended, plots with higher $^{143}Nd/^{144}Nd$ for a given $^{206}Pb/^{204}Pb$ relative to the crustal xenoliths. Interestingly, four samples (i.e. MN-30.5.1, MN-27.4 and the Gobi Altai rocks) are displaced toward the field for crustal xenoliths, suggesting crustal contamination may have affected these four samples. However, contradictory to this is that MN-30.5.1 and MN-27.4 contain mantle peridotite xenoliths; MN-27.4 also plots away from the crustal xenolith field on the plot of $^{143}Nd/^{144}Nd$ vs Nd (Fig. 10b). Thus, although crustal contamination may have affected the Gobi Altai samples, the majority of the Hangai lavas cannot be explained by bulk assimilation. Clearly, a much more varied suite of crustal xenoliths or more complex models for contamination would be required to explain all the data.

Assimilation–fractional crystallization (AFC) can be assessed using the equations presented by DePaolo (1981). The results of such modelling are shown in Fig. 10b, for different values of r, where r equals the rate of assimilation of wallrock/rate of fractionation. The AFC modelling curves were calculated using a bulk D value of 0·142 for Nd [calculated using distribution coefficients (D values) of 0·001 for olivine, 0·0068 for orthopyroxene, 0·14 for plagioclase, 0·087 for garnet and 0·44 for amphibole (McKenzie & O'Nions, 1995); 0·1873 for clinopyroxene (Hart & Dunn, 1993); and 0·01 for ilmenite and 0·01 for magnetite (Stimac & Hickmott, 1994), for a fractionating assemblage with hypothesized modal proportions of 15% olivine, 42% clinopyroxene, 33% plagioclase, 5% garnet, 2% ilmenite and 3% magnetite].

The modelling uses sample MN-25.1 as the parental magma composition, and is contaminated by a mid-crustal xenolith, 8531/44 [quartz (26·3%) + plagioclase (35%) + biotite (12%), muscovite (8%) + epidote (12·6%) + amphibole (5%) along with trace amounts of ilmenite and apatite; see Stosch *et al.* (1995) for further petrographic details for 8531/44]. Modelling of combinations of other parental magma compositions with different lower-crustal xenoliths reveals the same results as Fig. 10b, that only very high percentages of assimilation of crustal material can explain the isotopic variations. This seems to be highly unlikely given the major and trace element compositions of the basalts.

Isotopic and trace element data suggest that the role of crustal contamination has been negligible in the petrogenesis of the Mongolian basalt magmas. To further emphasize this point, we can examine the behaviour of trace element ratios. For example, both upper and lower crust are known to have low ratios of Ce/Pb (<5) and relatively high ratios of La/Nb ($\sim$1·5 and $\sim$4·5, respectively; Taylor & McClennan, 1985), whereas Ce/Pb

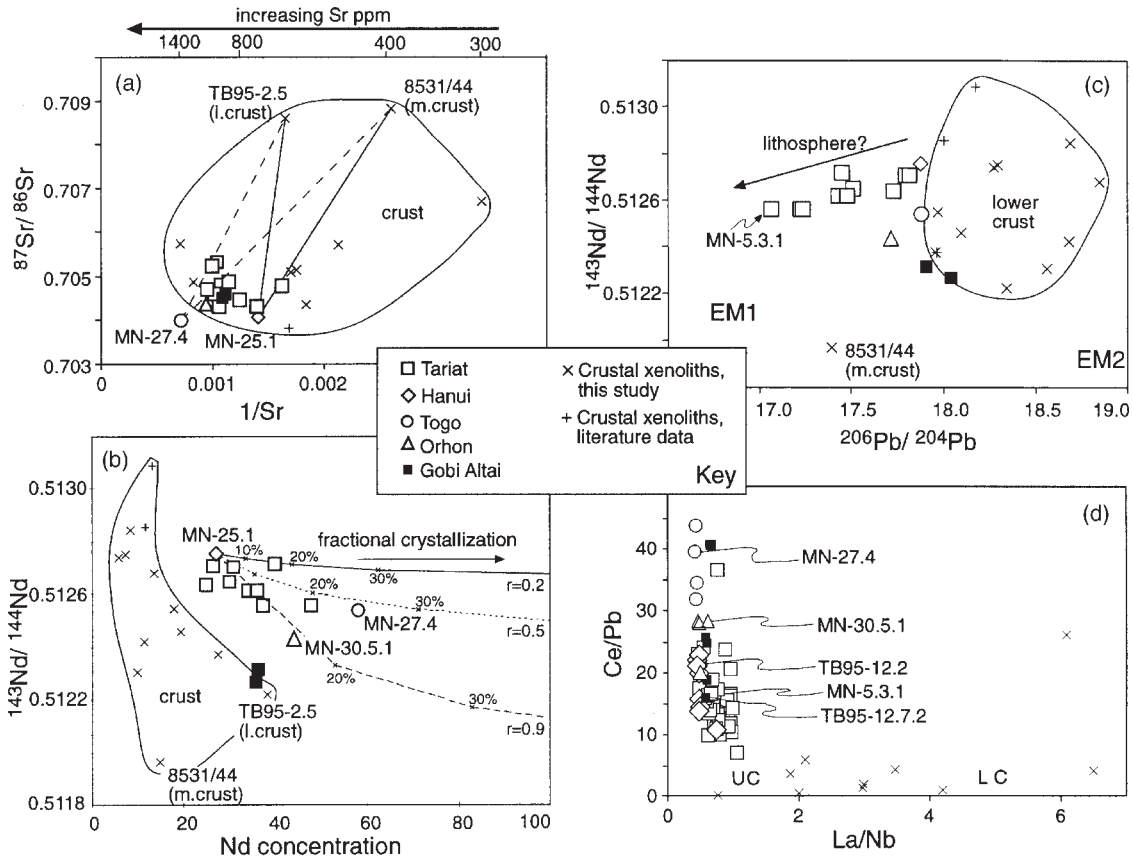

Fig. 10. (a) Plot of $^{87}Sr/^{86}Sr$ vs 1/Sr for basalts and crustal xenoliths. Lines are bulk mixing lines between two primitive Hangai samples [MN-25.1 (continuous lines) and MN-27.4 (dashed lines)] and two crustal xenoliths (TB95-2.5 and 8531/44). Field drawn around crustal xenolith data. Data sources: crustal xenoliths: Stosch *et al.* (1995). (b) Plot of $^{143}Nd/^{144}Nd$ vs Nd concentration (in ppm) with AFC modelling curves for different *r* values (where *r* is the rate of assimilation of wallrock/the rate of fractionation), at a bulk *D* value of 0·1389 [calculated for an assemblage with 20% ol, 15% cpx, 60% plag, 3% ilmenite and 2% magnetite, using the partition coefficients of Hart & Dunn (1993), Stimac & Hickmott (1994) and McKenzie & O'Nions (1995)]. AFC modelling uses equations from DePaolo (1981) for contamination of sample MN-25.1 from Hanui with crustal xenolith, 8531/44, from Tariat. Ticks at 10% intervals for percentage assimilated. Data source for crustal xenoliths: Stosch *et al.* (1995)—field drawn around crustal xenolith data. (c) $^{143}Nd/^{144}Nd$ vs $^{206}Pb/^{204}Pb$ for Mongolian basalts and crustal xenoliths. Data sources: crustal xenoliths: Stosch *et al.* (1995)—field drawn around crustal xenolith data; EM1 and EM2: Zindler & Hart (1986). (d) Ce/Pb vs La/Nb for all Mongolian basalt data and crustal xenoliths. Data source for upper crust (UC) and lower crust (LC): Taylor & McClennan (1985).

ratios for most mantle compositions are ~25 and primitive mantle ~9 (Hofmann *et al.*, 1986). The Mongolian basalts exhibit a wide range of Ce/Pb ratios, with most samples falling between 9·8 and 43·68 (Fig. 10d), and are therefore much more similar to mantle than crustal compositions. Crustal xenoliths from Mongolia have much higher La/Nb than the basalts, and interestingly, samples that appear to show evidence for crustal contamination in their isotopic compositions (e.g. MN-27.4, MN-30.5.1, TB95-12.2 and TB95-12.7.2) do not have significantly lower Ce/Pb or higher La/Nb than other Mongolian lavas (Fig. 10d; Table 3). In fact, MN-27.4 has the one of the lowest La/Nb and highest Ce/Pb compositions observed within the dataset (Fig. 10d).

To any significant extent, we cannot account for the observed isotopic and trace element variations by crustal contamination. In the next section, we discuss the possibility that the isotopic variations are due to interaction with, or derivation from, continental lithospheric mantle, and use the isotope and trace element data to infer the composition and nature of the mantle source.

Role of lithospheric mantle

Melting conditions: depth and degree of melting

If we accept that the Mongolian parental magmas have not been significantly affected by crustal contamination, then the range in isotopic and trace element compositions must have been acquired before reaching crustal levels, i.e. they were inherited through partial melting of a heterogeneous asthenospheric or lithospheric mantle

source(s) or through interaction of asthenosphere-derived magmas with the lithospheric mantle. The thickness of the Mongolian lithospheric mantle has been variably quoted between 50 and 150 km (Zorin, 1981; Kiselev, 1985; Delvaux, 1997). From an examination of the basalt geochemistry presented here we can assess the depth range from which these lavas formed.

REE patterns (Fig. 5) indicate that garnet influenced the variations in HREE, suggesting that the basalts originated from a garnet peridotite source. Detailed *P–T* estimates on garnet lherzolite xenoliths from Tariat indicate equilibration at 20·8 kbar, 1106°C, i.e. from ~70 km depth (Ionov *et al.*, 1998). Ionov *et al.* (1998) calculated that the garnet to spinel transition occurred over the pressure range of 20·8–18·3 kbar.

Using combined Hf isotope and Lu/Hf data, it is possible to place at least some constraints on the source mineralogies (Fig. 9b; see Beard & Johnson, 1993). This is because the partitioning systematics between melt and residual mantle for Lu and Hf are strongly affected by the presence of garnet. The low $^{176}Hf/^{177}Hf$ isotope ratios of the Mongolian basalts suggest low time-integrated Lu/Hf ratios in the mantle source; Lu/Hf values required range from 0·022 to 0·038, which are much lower than those for MORB-source mantle, indicating a relatively primitive or fertile source for the Mongolian lavas. This is consistent with the relatively fertile nature of some of the Mongolian mantle xenoliths (Ionov, 1986). Measured Lu/Hf vs Sm/Nd ratios (Fig. 9b) show a positive correlation and plot along a model curve for melts derived from a garnet-facies rather than spinel-facies peridotite mantle source.

In an attempt quantitatively to constrain the melting conditions, Fig. 11 shows the results of REE inversions (McKenzie & O'Nions, 1991, 1995) for 10 Tariat samples with MgO >6 wt %. The inversion models take REE concentrations in any given sample to estimate the melt fraction as a function of depth and total integrated melt fraction. The inversion modelling indicates that melting began beneath Tariat at depths of ~150 km and stopped at ~90 km, putting it entirely within the garnet stability field, and with an extent of partial melting as high as 12% (D. McKenzie, personal communication, 1998). Unfortunately, these figures do not constrain whether the melting was entirely within the lithosphere, the asthenosphere, or both; it may be recalled that the estimates of the thickness of the lithosphere beneath Mongolia vary from 50 to 150 km (Zorin, 1981; Kiselev, 1985; Delvaux, 1997). None the less, these calculations constrain the depth of melting to be within a garnet-peridotite source at a depth of >70 km.

Given that melting occurred at depths >70 km, and that the extent of melting was unlikely to remain constant through time, how much can we determine about the relative degree of melting? Making the broad assumption that the more undersaturated a melt is, the smaller the degree of partial melting (e.g. Frey *et al.*, 1978) we can assess relative degrees of melting. Figure 12 shows the saturation index (SI) for lavas from Gobi Altai and Tariat arranged in approximate chronological order. It should be noted that the stratigraphy within each province is only approximate and based predominantly on field relationships. Owing to a lack of stratigraphic correlations between individual volcanic provinces, Hanui, Togo and Orhon are not included in this diagram because their timing cannot be integrated with that of the Tariat lavas.

We can see from Fig. 12 that the samples from Gobi Altai have uniformly low SI values, consistent with small degrees of melting. The oldest Tariat lavas also exhibit low SI values, consistent with similarly small amounts of melting. Younger rocks from Tariat are generally more Si saturated, consistent with generally higher degrees of partial melting. However, a return to undersaturated melts is observed again in the youngest rocks from Tariat, indicating small-degree melts. This suggests that throughout the Cenozoic, magmatism was largely confined to small-volume, small-degree partial melts. Even during the period of maximum volcanism, i.e. within the period ~5–6 Myr ago, the volumes of magma erupted are not exceptionally large, as might be expected if associated with a mantle plume.

In summary, there is no clear indication of a change in depth, i.e. from garnet- to spinel-facies mantle, as might be expected for an actively upwelling plume system (e.g. Ethiopia; Pik *et al.*, 1999), nor is there any dramatic change in the degree of partial melting, as might be expected for a dynamic mantle plume, potentially increasing to very large degrees of partial melting. Geochemical evidence indicates that, on average, the Mongolian lavas were generated by small degrees of partial melting within the garnet stability field. This contrasts with the most abundant xenolith population that has been retrieved from Mongolian Cenozoic basalts, which are most commonly spinel peridotites. This suggests that melting is likely to have occurred close to the base of the lithosphere, or was even sub-lithospheric.

Source heterogeneity and the role of accessory mineral phases

The majority of the mantle xenoliths entrained by Cenozoic basalts in Mongolia and nearby Lake Baikal in Russia are compositionally variable and anhydrous; relatively fertile spinel and garnet + spinel lherzolites occur most commonly, but also present are spinel and garnet + spinel pyroxenites, harzburgites and spinel websterites (Kepezhinskas, 1979; Ionov, 1986; Preß *et al.*, 1986; Stosch *et al.*, 1986, 1995; Genshaft & Saltykovskiy, 1987; Harmon *et al.*, 1987; Stosch, 1987; Kopylova *et al.*, 1990, 1995; Ionov & Wood, 1992; Ionov *et al.*, 1992, 1994, 1995, 1999). Rarely xenoliths containing

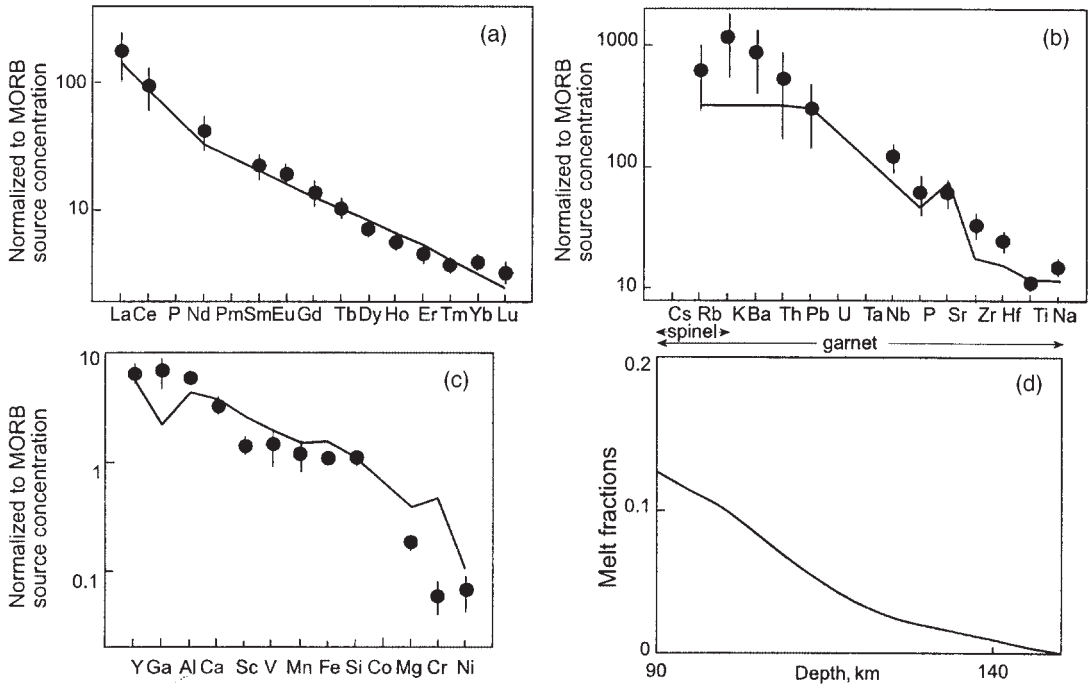

Fig. 11. Results of inversion modelling of Hangai basalts from Tariat following the method of McKenzie & O'Nions (1991, 1995). Predicted concentrations from the modelling for: (a) REE; (b) other minor and trace element concentrations; (c) major and transitional elements; all data normalized to MORB source concentrations (given by Tainton & McKenzie, 1994). ●, mean observed elemental concentrations in the basalts with range given. (d) Melt distribution for the elemental concentrations in (a) shown by continuous curve (see McKenzie & O'Nions, 1991).

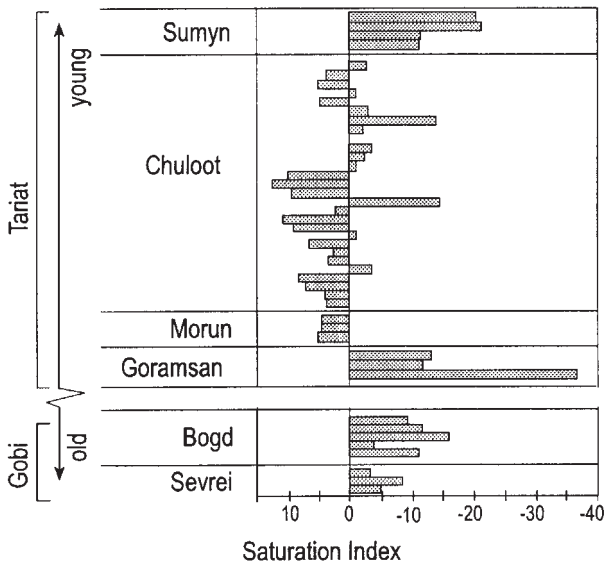

Fig. 12. Saturation index for all Tariat and Gobi Altai samples plotted in estimated chronological order. (It should be noted that Hanui, Orhon and Togo are not shown because of uncertainties about their stratigraphic relationships relative to Tariat). Saturation Index = 100 × [Si − (Al + Fe^{2+} + Mg + 3Ca + 11Na + 11K + Mn − Fe^{3+} − Ti − 4P)/2], where Si, Al, etc. are wt % oxide/molecular weight of the oxide (Fitton *et al.*, 1991).

phlogopite and amphibole occur, which are indicative of metasomatic enrichment (Stosch *et al.*, 1986; Ionov *et al.*, 1994, 1999).

Recent work has shown that some basalt-hosted mantle xenoliths from Siberia preserve evidence of an unusual multi-stage metasomatic history, in which amphibole and mica from an earlier metasomatic episode are replaced during influx of later metasomatic melts by feldspar-rich and Ti-oxide aggregates (Ionov *et al.*, 1999). These pseudomorphed minerals are enriched in incompatible elements; in particular the Ti-rich oxide minerals, which include rutile, ilmenite and even armalcolite, are rich in Nb and Zr (Ionov *et al.*, 1999). These minerals are rare in most mantle xenolith suites, but notably are observed in harzburgite xenoliths from Kerguelen (Ionov *et al.*, 1999). The unusual composition of these metasomatically altered xenoliths is inferred to be a response to alkali-rich fluids and melts with low water activity percolating through the lithosphere from the asthenosphere, and not from subducted crustal sources (Ionov *et al.*, 1999); in the case of Kerguelen this suggests mantle plume activity.

Ilmenite xenocrysts occur within some of the Mongolian lavas, especially those from Togo and the Bogd Plateau. Although little is known about their original petrological assemblage (they are not observed in association with any other mineral phase), their presence suggests that their host lavas may have interacted with

metasomatized lithospheric mantle. Consequently, we investigate the role of metasomatized lithosphere with regard to the genesis of the Mongolian lavas, and assess the possible contribution from hydrous phases during partial melting.

Partial melting of a hydrous phase

Normalized trace element distribution patterns exhibit positive anomalies at K, Nb, Sr and P, suggesting that hydrous minerals and apatite have contributed to the petrogenesis of the primary magmas (Fig. 5). Mantle amphibole crystallizes early from metasomatic melts and begins to melt close to solidus temperatures (Greenough, 1988). Melting of amphibole or phlogopite will enrich the melt in K and other LILE (e.g. Sr from amphibole and Rb and Ba from phlogopite), if the melt fraction is sufficiently high for minerals to be completely consumed during the melting process. Niobium, being more compatible in amphibole than in any other silicate mineral in mantle peridotite, is a good indicator for the presence of amphibole in the source region (McKenzie & O'Nions, 1995; Tiepolo *et al.*, 2000). It should be noted, however, that this statement may be complicated by the presence of Ti-rich oxide minerals in the lithospheric mantle; the high Nb content of the Togo basalts may be an indication that Ti-rich oxide minerals contributed to the melt composition.

To test the hypothesis that hydrous minerals contributed to the primitive basalt magma compositions within Mongolia, petrogenetic models have been constructed to simulate melting of a hypothetically enriched lithospheric mantle source composition. For this purpose we simulated an enriched mantle source by extracting 100 individual small melt fractions [of $F = 0{\cdot}001$, where F is the weight fraction of the melt produced from a batch melt, according to the equation of Hanson & Langmuir (1978), which is given below], of a primitive mantle source composition (Sun & McDonough, 1989) and adding those small melt fractions back to an original primitive mantle source composition.

Hanson & Langmuir (1978) formulated the following equation for simple batch melting:

$$C_L/C_O = 1/[D_O + F(1 - P)] \quad (1)$$

where C_L is the concentration of a trace element in the melt, C_O is the concentration of a trace element in the unmelted source, D_O is the bulk distribution coefficient at the onset of melting, calculated from

$$D_O = \Sigma Kd_j^i.W_j \quad (2)$$

where Kd is the partition coefficient for element i in mineral j and W is the proportion of mineral j in the source, F is the weight fraction of melt produced and P is the bulk distribution coefficient of the minerals that constitute the melt, where

$$P = p_1Kd_1 + p_2Kd_2 + p_3Kd_3 + \ldots \quad (3)$$

where p_x is the normative weight fraction of mineral x ($x = 1, 2, 3, ...$) entering the melt and Kd_x is the mineral–melt distribution coefficient for a given trace element for mineral x. Distribution coefficients used throughout this modelling are given in Table 5.

Starting with our hypothetically enriched source composition with a peridotite modal mineralogy of 0·6 ol, 0·15 cpx, 0·2 opx and 0·05 gt, with $p = 0{\cdot}4$, 0·3, 0·1 and 0·2, respectively, and using the simple batch melting equations of Hanson & Langmuir (1978), the predicted composition of partial melts of this enriched source will exhibit incremental LREE enrichment with decreasing degrees of melting with little variation in HREE concentrations. Such normalized REE patterns of variable LREE enrichment about fixed HREE concentrations are not observed in the Mongolian basalt samples. This is not, however, surprising, because the samples are unlikely to represent individual melt batches from a fixed depth or degree of partial melting, nor are likely to represent immediate extraction from the source region, which is implied by the batch melting equations. Instead, melting is probably continuous over a range of depths within the garnet stability field.

We therefore model a process of continuous melting accompanied by localized source re-enrichment. The model envisages a process whereby melt is extracted by the parameters set by batch melting, and the residual after melt extraction is calculated by

$$C_S/C_O = D_{RS}/[D_{RS} + F(1 - D_{RS})] \quad (4)$$

[Rollinson (1993), adapted from Hertogen & Gijbels (1976)], where C_S is the concentration of a trace element in the unmelted residue and D_{RS} is the bulk partition coefficient of the residual solid. A melt (L_1) calculated to form at $F = 0{\cdot}001$, i.e. small degrees of partial melting (other F values shown in Fig. 13 for comparison) is extracted from C_O, the original mantle source, whereupon it infiltrates overlying mantle (C_O^1), causing enrichment of mantle source C_O^1. Melting is then modelled to occur at a higher degree of partial melting ($F = 0{\cdot}002$) as a result of its supposedly shallower depth with the new melt from C_O^1 (L_2; Fig. 13) being extracted from its residue and subsequently infiltrating unmodified overlying mantle (C_O^2), and so on.

The melting model attempts to address some of the processes by which melt is extracted from its residual mantle and interacts with overlying fertile mantle similar to that defined by zone refining. As a result of surface tension effects around individual crystals, complete melt extraction from any given source will not be possible,

Table 5: Partition coefficients used for melting model calculations

	Ol	Cpx	Opx	Gt	Amph	Phlog
Ba	0·0003	0·0005	0·0001	0·0005	0·76	1·09
Rb	0·00018	0·001	0·0006	0·0007	0·2	3·06
K	0·00018	0·002	0·001	0·001	1·2	3·67
Nb	0·005	0·02	0·005	0·07	0·8	0·088
La	0·0004	0·054	0·002	0·01	0·17	0·028
Ce	0·0005	0·098	0·003	0·021	0·26	0·034
Nd	0·001	0·21	0·0068	0·087	0·44	0·032
Sm	0·0013	0·26	0·01	0·217	0·76	0·031
Zr	0·01	0·1	0·03	0·32	0·5	0·6
Eu	0·0016	0·31	0·013	0·32	0·88	0·03
Gd	0·0015	0·3	0·016	0·498	0·86	0·03
Tb	0·0015	0·31	0·019	0·75	0·83	0·03
Dy	0·0017	0·33	0·022	1·06	0·78	0·03
Ho	0·0016	0·31	0·026	1·53	0·73	0·03
Er	0·0015	0·30	0·03	2·00	0·68	0·034
Yb	0·0015	0·28	0·049	4·03	0·59	0·042
Lu	0·0015	0·28	0·06	5·5	0·51	0·046

D values for Ol, Cpx, Opx, Plag, Gt and Amph from McKenzie & O'Nions (1995); Phlog from Rollinson (1993, and references therein) and La Tourrette *et al.* (1995); Ho and Tb speculated from the partition coefficients values of elements adjacent to them. It should be noted that no account has been made for variance in partition coefficients as a result of temperature and pressure.

therefore a 'correction' has been written into the calculation for an arbitrary 1% of the melt to remain in each residual source (this is probably unrealistically low for very small degrees of partial melting, where a greater percentage of the melt will be affected by surface tension around crystals than for a higher-degree melt, but the same value has been used throughout for consistency).

To determine modal proportions of mineral phases within each source mineral assemblage, account must be given for the loss of a percentage of minerals from the source region to make up the melt chemistry. The mineral assemblage in the residue will be different, depending on the value of p, where p is the normative weight fraction of mineral in the melt. The new modal proportions of the mineral phases given as W_{new} can be calculated from

$$W_{new} = \frac{W_{old} - Fp}{(1 - F)} \quad (5)$$

where W is the proportion of a given mineral in the source and F is the weight fraction of the melt produced.

The melting model calculations can be repeated until elemental concentrations or a mineral phase become exhausted. In the calculations undertaken in this study, some elements become exhausted before mineral phases. These calculations are similar to zone refining melting processes, and indeed the same calculations can be made using zone refining equations. However, we have used batch melting equations because it is a simpler process to model, and the only significant difference in using zone refining equations is that LILE enrichment is greatly enhanced relative to other elemental enrichment and therefore calculations cannot be repeated so many times before LILE concentrations become exhausted. Similar models, e.g. dynamic melting (Langmuir *et al.*, 1977), have attempted to take account of the continuum nature of a melt column originating within a homogeneous mantle source. Unfortunately, the dynamic melting model cannot be applied to the Mongolian mantle source region because of its likely heterogeneity.

Melting models for two source compositions are calculated, one containing amphibole (model A; Fig. 13a) and the other containing both amphibole and phlogopite (model B; Fig. 13b). The initial modal proportions of the starting compositions for models A and B are given in Table 6. Results for model A show that Nb is strongly retained in the residue during the first melting steps, but melts produced from C_O^2 (L_3; Fig. 13a), particularly higher-degree partial melts, appear to be similar to average Tariat compositions. For melting model B, with a source containing modal amphibole and phlogopite, LILE enrichment is much greater than in model A and shows that although absolute values in these models may

not be realistic, and indeed could vary according to different published partition coefficients, the former of the two melting models shows greater similarity to the mantle-normalized trace element patterns of the Tariat basalts.

In summary, the compositions of the Mongolian basalts appear to reflect derivation from a source containing amphibole and garnet, and in some cases perhaps minor amounts of phlogopite. Phlogopite megacrysts have been found in some basalts, not analysed in this study, from the Tariat province (Barry, 1999). Initial enrichment of the mantle source region may have taken place by infiltration of asthenospheric melts, with subsequent re-melting causing progressive advancement of melts within the lithospheric mantle, i.e. enrichment by a 'chromatographic'-type process (e.g. Navon & Stolper, 1987). A metasomatically enriched hydrous source, similar to that proposed here, has been inferred for some Eastern Australian basalts rich in Nb, but low in K and Rb (O'Reilly & Zhang, 1995; Zhang *et al.*, 1999). Negative K, P and Sr anomalies in the Australian basalts have been attributed to the presence of residual amphibole and apatite in the mantle source (O'Reilly & Zhang, 1995; Zhang *et al.*, 1999). However, in the context of the Mongolian basalts, positive anomalies of K, Nb, Sr and P (Fig. 5) can be explained by melting a source region that had hydrous phases present but insufficiently abundant to be residual after relatively low degrees of partial melting. Tiepolo *et al.* (2000) pointed out that vein amphiboles in equilibrium with mantle peridotite may have higher Nb contents than disseminated equivalents, therefore suggesting that the hydrous phases contributing to the Mongolian magmatism may have existed as veins.

Timing of metasomatic enrichment

Near Mongolia, in the Vitim volcanic field of Siberia, metasomatic enrichment of the lithospheric mantle apparently occurred immediately before xenolith entrainment (Litasov *et al.*, 2000) and in Dariganga, SE Mongolia (Fig. 1b), a melt infiltration event appears to have been synchronous with recent volcanism (Ionov *et al.*, 1994). However, the timing of metasomatic enrichment elsewhere in Mongolia is less clear. Metasomatic enrichment beneath Mongolia is unlikely to be ancient because the $^{87}Sr/^{86}Sr$ ratios are not particularly elevated and subduction-related enrichment during Upper Proterozoic to Palaeozoic arc amalgamation (e.g. Sengör & Natal'in, 1996) does not present a potential mechanism for enrichment of the lithospheric mantle because there is no indication of a subduction signature in the xenoliths or the lavas.

Other processes that may cause metasomatic enrichment include: (1) recent infiltration of aqueous or carbonate fluids or silicate melts above a thermal anomaly; (2) enrichment as a result of older magmatic events, e.g. Mesozoic magmatism. In view of the evidence against the involvement of a high heat flux mantle plume, explanation for enrichment by recent processes is problematic unless a smaller thermal anomaly could account for continual melt percolation into the lithosphere (Barry, 1999). Enrichment owing to older magmatic events appears unable to explain enrichment in central Mongolia because Mesozoic volcanic rocks are observed only in southern and eastern Mongolia, not in Hangai. However, from evidence provided by lower-crustal xenoliths from Tariat, basaltic underplating has occurred and the timing of this is unknown. Therefore neither cause of enrichment can be ruled out at present.

Source characteristics, implications for chemical reservoirs: isotopic end-members in the Mongolian basalts

The data presented in Figs 7–9 show that the Mongolian basalts are isotopically heterogeneous, and, given the lack of evidence for significant crustal contamination, suggest mantle source heterogeneity or mixing of melts derived from different mantle reservoirs. The Hangai samples can be explained by mixing two end-member sources, but a third component is required to explain the Gobi Altai samples.

One end-member has $^{206}Pb/^{204}Pb > \sim 17{\cdot}8$, and Nd, Hf and Sr isotope compositions close to, or more depleted than, BSE. This component is characterized by samples from Tariat and Hanui. The second end-member composition is characterized by low $^{206}Pb/^{204}Pb$, but relatively high $^{207}Pb/^{204}Pb$ for a given $^{206}Pb/^{204}Pb$ ratio, Nd and Sr isotope compositions close to BSE, and low Hf isotope ratios. This component is best represented by young samples from Tariat, e.g. MN-5.3.1. This component is clearly not normal MORB-source asthenosphere. Neither is it crustal in origin because (1) at least some of the Mongolian lavas with this type of composition (e.g. MN-5.3.1) are rich in mantle xenoliths (Table 1) and (2) it is unlike measured crustal xenolith compositions (Figs 7 and 8). Similarly, there are problems in attributing this component to present-day lithospheric mantle, as represented by entrained mantle xenoliths from Mongolia and China, as it plots outside their isotopic field (Figs 7 and 8). Rather than present-day lithosphere, it may represent old lithosphere that has become detached or a component introduced into the area by mantle convection.

Possibly the greatest similarity of this low $^{206}Pb/^{204}Pb$ component is with EMI, as seen elsewhere in NE China (Tatsumoto *et al.*, 1992) and some Indian mid-ocean ridge basalts (Fig. 8). It is also widely recognized in continental and marginal basin basalts from east and SE Asia (Hickey-Vargas *et al.*, 1995; Pearce *et al.*, 1999) as

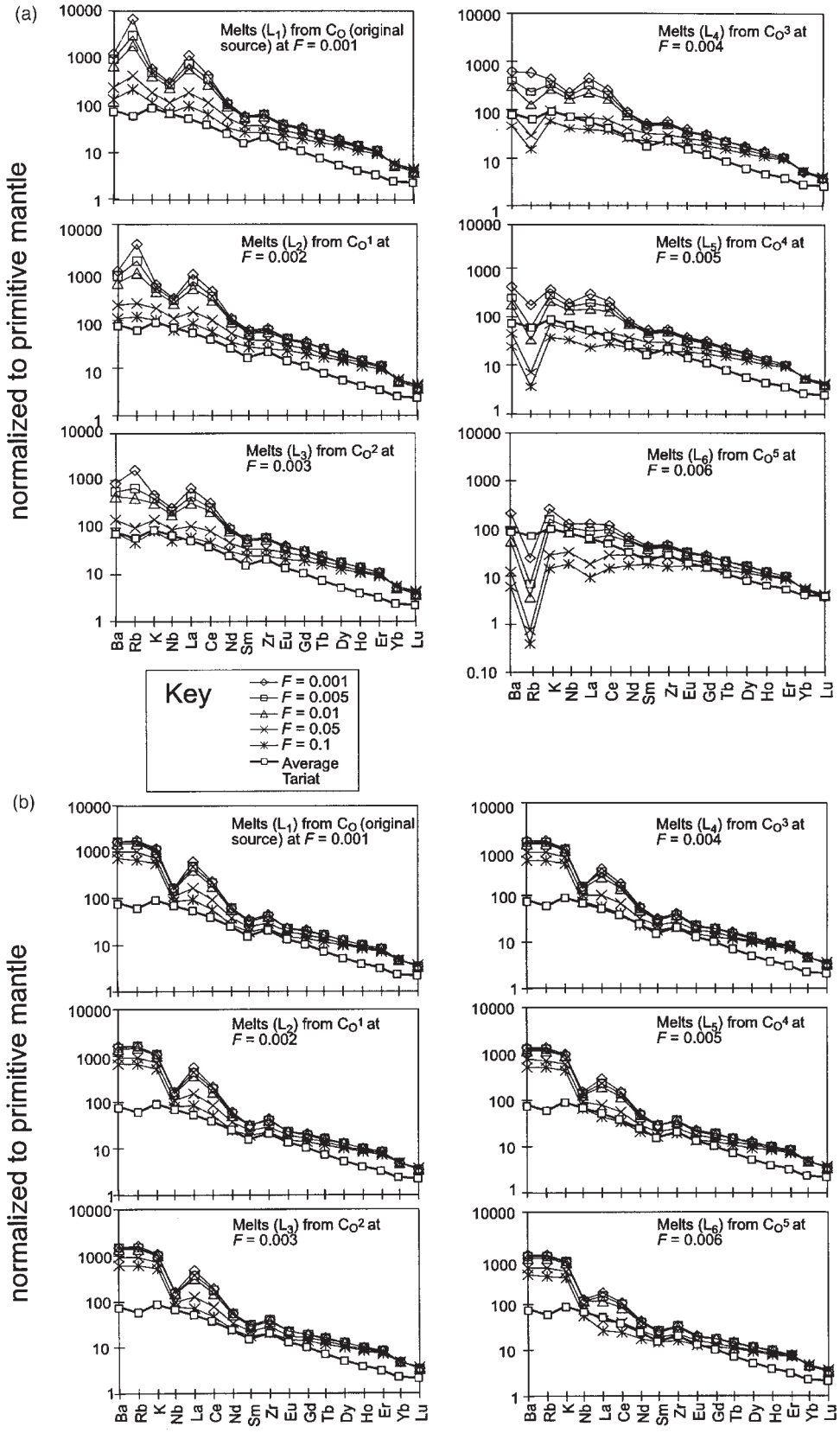
(a)
normalized to primitive mantle
Melts (L_1) from C_O (original source) at F = 0.001
Melts (L_2) from C_O^1 at F = 0.002
Melts (L_3) from C_O^2 at F = 0.003
Melts (L_4) from C_O^3 at F = 0.004
Melts (L_5) from C_O^4 at F = 0.005
Melts (L_6) from C_O^5 at F = 0.006
Ba Rb K Nb La Ce Nd Sm Zr Eu Gd Tb Dy Ho Er Yb Lu
Key
F = 0.001
F = 0.005
F = 0.01
F = 0.05
F = 0.1
Average Tariat
(b)
normalized to primitive mantle
Melts (L_1) from C_O (original source) at F = 0.001
Melts (L_2) from C_O^1 at F = 0.002
Melts (L_3) from C_O^2 at F = 0.003
Melts (L_4) from C_O^3 at F = 0.004
Melts (L_5) from C_O^4 at F = 0.005
Melts (L_6) from C_O^5 at F = 0.006
Ba Rb K Nb La Ce Nd Sm Zr Eu Gd Tb Dy Ho Er Yb Lu

Table 6: Initial modal proportions of the starting compositions for melting models A and B

	W: melting model A	*W*: melting model B	*p*: melting model A	*p*: melting model B
Olivine	0·55	0·55	0·05	0·05
Clinopyroxene	0·15	0·15	0·3	0·2
Orthopyroxene	0·22	0·2	0·05	0·05
Garnet	0·05	0·05	0·2	0·2
Amphibole	0·01	0·04	0·4	0·4
Phlogopite	—	0·01	—	0·1
Total	1·00	1·00	1·00	1·00

Definitions of *p* and *W* are given in the text.

well as Taiwan (Chung *et al.*, 1994). Tu *et al.* (1992) and Flower *et al.* (1992) described localized, or 'endogenous', Dupal-like mantle in the South China Basin and attributed its presence to mixing caused by lithospheric extension associated with the India–Asia collision.

A third component is characterized by low $^{143}Nd/^{144}Nd$ and lower $^{207}Pb/^{204}Pb$ ratios than other Mongolian basalts for a given $^{206}Pb/^{204}Pb$ ratio. This component is observed only in samples from Orhon and the Gobi Altai, and, with regard to the Pb-isotope composition, shows similarity to EM2. However, an EM2-type composition is not evident from the $^{143}Nd/^{144}Nd$ isotope data, which appear to trend towards EM1 (Figs 7 and 8).

The origin of EM1-type compositions remains controversial, but has generally been attributed to either: (1) contamination of the asthenosphere by either deep mantle plumes (Storey *et al.*, 1988) or ancient subducted recycled sediments (Rehkämper & Hofmann, 1997); or (2) continental mantle lithosphere delamination during continental break-up (Mahoney *et al.*, 1992). Ce/Pb systematics rule out recycled sediments or a role for subduction (Fig. 10d), and a deep mantle plume model, as discussed, lacks supportive evidence. Therefore, the involvement of EM1 must be accounted for either by a thermal anomaly or by a model of lithospheric weakening or delamination coupled with replacement by asthenospheric melts.

A model for Mongolian magmatism: implications for continental alkalic volcanism

This section considers the possible causes of Mongolian magmatism within the context of the tectonic setting and Cenozoic magmatic history of NE Asia. There are several similarities between the Cenozoic magmatism in Mongolia and that throughout NE China and Siberia (Barry & Kent, 1998). Furthermore, diffuse volcanism throughout much of Asia appears to have begun around the mid-Miocene, posing the question of whether there has been a common process acting upon the whole of eastern Asia. The discussion of such regional volcanism has implications for understanding other global examples of small-scale, diffuse, intra-continental alkalic volcanism, where there is no obvious cause of volcanism. In the absence of positive evidence for a high heat flux mantle plume or substantial regional lithospheric extension, an alternative mechanism for mantle melting is sought. It is a non-trivial problem to explain the source of energy that enables deep melting to occur, and is a relevant issue for other cases of continental magmatism such as in central Europe (see Wilson & Patterson, 2001).

We have shown that the Mongolian basalt melts equilibrated, at least in part, within the garnet stability field, and possibly at depths >120 km. Under anhydrous melting conditions, this requires a potential temperature far in excess of the ambient asthenospheric mantle potential temperature (~1300°C; McKenzie & Bickle, 1988). However, volatile-present melting will lower the solidus temperature of the mantle; mantle amphiboles, such as pargasite and kaersutite, melt under water-undersaturated conditions at ~1140°C at pressures >25 kbar (Mengel & Green, 1989). As discussed, the geochemical evidence from the Mongolian basalts is that they are likely to have formed under such conditions.

Assuming a model of basalt petrogenesis from an amphibole-bearing garnet peridotite source, there remain two issues: how the metasomatic enrichment occurred, and the implications of partial melting of metasomatized lithosphere for mantle potential temperatures. As discussed above, the timing of the metasomatic enrichment is unknown, and could be attributed to either (1) melts mobilized by a thermal anomaly during the Cenozoic era, or (2) Mesozoic magmatic activity, which could have enriched the lithospheric mantle.

Fig. 13 (opposite). Primitive mantle-normalized trace element distribution patterns for partial melts of an enriched mantle source with (a) 0·01% modal proportion of amphibole (model A) and (b) 0·01% modal proportion of phlogopite and 0·04% modal proportion of amphibole (model B). Individual primitive mantle-normalized trace element distribution patterns are for successive melt extraction events in a dynamic decompressive system with melts formed at different values of *F* (representing different degrees of partial melting, i.e. weight fractions of melt produced), from each progressively enriched source region. Detail of calculation parameters given in text.

Model 1

If we explore the first model, metasomatism may have occurred as a multi-stage process of melt infiltration from the asthenosphere. However, as Wilson *et al.* (1995) pointed out, such melts must be derived from a fertile mantle source, because the isotope geochemistry of the magmas cannot be explained by small-degree melts of depleted MORB-source mantle. The cause of a thermal anomaly remains enigmatic. If Mongolia and neighbouring regions are underlain by hotter than ambient temperature mantle, but not underlain by a detectable deeply rooted, high heat flux mantle plume at the present, there appear to be three explanations for excess thermal energy, as follows.

(1) A mantle plume, complete with a deeply rooted stem, was active during the earliest phase of magmatism but has now waned; the stem has disappeared, and only a cooling lens of mantle remains under Mongolia. This may explain the presence of shallow anomalous mantle material imaged beneath Hangai by Petit *et al.* (2002), but it begs the question of what caused similar volcanic activity in other regions of Asia. Furthermore, the absence of a significant temporal variation in the volume of magmatic activity also suggests that this is not the correct model (we might expect activity to have been more voluminous in the early history of the mantle plume).

(2) A deep, active mantle plume may be situated beneath the Asian continent and feeds material laterally into thin spots (Thompson & Gibson, 1991) on the base of the Mongolian lithosphere or supplies smaller 'fingers' of hot material (see Wilson & Patterson, 2001) to the base of the lithosphere. Unfortunately, there are insufficient high-resolution seismic tomography data to fully test this. However, for this model to be viable, the plume must have been active at least for the past 30 Myr to explain the longevity of the magmatism. If correct, this model can explain regional warming of the asthenospheric mantle and emplacement of a thermal anomaly laterally beneath Mongolia, leading to magmatism in focused zones.

(3) The Eurasian continent may be acting as a thermal blanket, and the upper mantle is slowly warming in response to convection from the 670 km discontinuity. Whether or not the convection systems associated with this type of process have the aspect of focused plumes, or broad cells (e.g. Anderson et al., 1992), is debatable. This process can also explain progressive warming of the lithosphere leading to partial melting of lower solidus domains.

Model 2

We can consider the second possible cause of metasomatic enrichment, that of Mesozoic magmatic activity. Metasomatism throughout the Mesozoic may have structurally weakened the Mongolian lithosphere, potentially causing small-scale lower-lithosphere delamination or replacement by asthenospheric mantle when Cenozoic tectonic stresses began to affect the Mongolian lithosphere. There is no positive evidence for lithospheric thinning; however, seismic and xenolith evidence suggests that asthenospheric material intrudes into the lowermost lithosphere beneath Mongolia (Ionov *et al.*, 1998; Kozhevnikov, 1999). A model of delamination could explain the unusual occurrence of doming in the Hangai region with localized, buoyant, hot asthenospheric material enveloping delaminated lithosphere (see Cunningham, 2001). This model has the added attraction of explaining why the deepest rift on Earth, Lake Baikal, has no volcanism within the rift, yet nearby there are volcanic provinces such as Vitim, Hamar-Daban and Bartoy. Models of lower-lithosphere delamination, in response to tectonic stresses, have been proposed elsewhere in Asia to explain diffuse Cenozoic basalts provinces, e.g. NE China (Menzies *et al.*, 1993; Flower *et al.*, 1998) and Vietnam (Nguyen *et al.*, 1996; Hoang & Flower, 1998).

At this stage, we are unable to constrain whether infiltration of asthenospheric material into the lithosphere beneath Mongolia is due to (1) a thermal anomaly feeding material into thinspots laterally or (2) lithospheric delamination. Of course, these are two end-members and could be combined in a scenario whereby structurally weakened lithosphere is impinged by mantle of hotter than ambient potential temperature. Both models could account for the involvement of a low $^{206}Pb/^{204}Pb$ component that may characterize the Asian asthenosphere. This component does not appear to be present within the portion of the lithospheric mantle sampled by the fertile mantle xenoliths; these may represent fragments of recently accreted lithosphere. Instead, a low $^{206}Pb/^{204}Pb$ component may reside in old lithosphere ($\sim$2 Ga) from the time of crustal stabilization (Kovalenko *et al.*, 1990). In the future, it may be possible to distinguish between the two proposed models, perhaps with the aid of higher-resolution tomographic imaging, better understanding of the timing of metasomatism, and maybe helium isotope studies, although a thermal anomaly may not be chemically distinct.

CONCLUSIONS

(1) Applying constraints provided by new crustal xenolith data, we can determine that crustal contamination has not influenced basalts from Mongolia sufficiently to affect their trace element and Sr–Nd–Pb–Hf isotopic ratios.

(2) Modelling of trace element data suggests that the Mongolian basalts were generated by small degrees of partial melting of an amphibole-bearing garnet peridotite source, at depths >70 km. The extent of partial melting

appears to have remained much the same throughout the >30 Myr of Cenozoic volcanic activity in Mongolia.

(3) Isotopic evidence suggests the involvement of at least three source components to explain the array of data observed in the Mongolian basalts. The first has $^{206}Pb/^{204}Pb > \sim 17{\cdot}8$, and Nd, Hf and Sr isotope compositions similar to BSE. This component most probably resides in the shallow asthenosphere. The second component is characterized by low $^{206}Pb/^{204}Pb$, but relatively high $^{207}Pb/^{204}Pb$ for a given $^{206}Pb/^{204}Pb$ ratio, and $^{143}Nd/^{144}Nd$ and $^{87}Sr/^{86}Sr$ close to BSE. This component shows some similarity to EM1 and may represent mobilized ancient lithospheric mantle. The third component, which appears to show isotopic decoupling, indicates a complicated enrichment history. It is characterized by low $^{143}Nd/^{144}Nd$ and low $^{207}Pb/^{204}Pb$. It most probably originates within the lithospheric mantle, and shows some similarities to EM2. It is predominantly sampled within the Gobi Altai, the oldest basalts sampled during this study.

(4) Contrary to many previous models, high heat flux mantle plume melting of anhydrous asthenosphere is not required to explain the Cenozoic Mongolian magmatism. Instead, the magmatism can be explained by a process of metasomatic enrichment of the lower lithosphere, followed by subsequent melting of the enriched mantle domains, which could have been triggered by a low heat flux thermal anomaly, either fed laterally from a mantle upwelling or caused by thermal blanketing of the large Asian landmass causing melting of sub-lithospheric mantle regions, or alternatively by replacement or delamination of the lowermost lithosphere in response to tectonic stresses. At this stage neither model is preferred, though increasing geophysical data may lend greater support to a thermal anomaly model.

ACKNOWLEDGEMENTS

We thank G. Badamgarov and Otgon for field assistance in Mongolia, and D. Cunningham for helping with field studies. We also thank H.-G. Stosch for donating crustal xenoliths for further analysis; S. Goldsmith and L. Coogan for ICP-MS analysis at Cardiff University; K. Jarvis and L. Clarke at Silwood Park, Ascot; and D. McKenzie for the rare earth inversions. The manuscript has been greatly improved thanks to the helpful, constructive comments of reviewers G. Morris and W. Bohrson, and special thanks go to M. Wilson for such painstaking, thorough reviews and thoughtful comments. This work was supported by NERC studentship GT4/95/155/E and is NIGL Publication 507.

SUPPLEMENTARY DATA

Supplementary data are available on *Journal of Petrology* online.

REFERENCES

Albarède, F. (1995). Residence time analysis of geochemical fluctuations in volcanic series. *Geochimica et Cosmochimica Acta* **57**, 615–621.

Anderson, D. L., Zhang, Y.-S. & Tanimoto, T. (1992). Plume heads, continental lithosphere, flood basalts and tomography. In: Storey, B. C., Alabaster, T. & Pankhurst, R. J. (eds) *Magmatism and the Causes of Continental Break-up. Geological Society, London, Special Publications* **68**, 99–124.

Arndt, N. T. & Christensen, U. (1992). The role of lithospheric mantle in continental flood volcanism: thermal and geochemical constraints. *Journal of Geophysical Research* **97**, 10967–10981.

Bach, W., Hegner, E., Erzinger, J. & Satir, M. (1994). Chemical and isotopic variations along the superfast spreading East Pacific Rise from 6°S to 30°S. *Contributions to Mineralogy and Petrology* **116**, 365–380.

Barry, T. L. (1999). Origins of Cenozoic basalts in Mongolia; a chemical and isotope study. Ph.D. thesis, University of Leicester, Leicester, 240 pp.

Barry, T. L. & Kent, R. W. (1998). Cenozoic magmatism in Mongolia and the origin of central and east Asian basalts. In: Flower, M., Chung, S.-L., Lo, C.-H. & Lee, T.-Y. (eds) *Mantle Dynamics and Plate Interactions in East Asia. American Geophysical Union Monograph, Geodynamics Series* **27**, 347–364.

Barsbold, R. & Dorjnamjaa, D. (1993). Geologic map of the Hangay Highland, 1:500 000. Ulaan Baatar: State Geological Centre.

Basu, A. R., Wang, J. W., Huang, W. K., Xie, G. H. & Tatsumoto, M. (1991). Major element, REE and Pb, Nd and Sr isotopic geochemistry of Cenozoic volcanic rocks of eastern China: implications for their origin from sub-oceanic-type mantle reservoirs. *Earth and Planetary Science Letters* **105**, 149–169.

Beard, B. L. & Johnson, C. M. (1993). Hf isotope composition of Late Cenozoic basaltic rocks from northwestern Colorado, USA: new constraints on mantle enrichment processes. *Earth and Planetary Science Letters* **119**, 495–509.

Bohrson, W. A. & Spera, F. J. (2001). Energy-constrained open-system magmatic processes II: Application of energy-constrained assimilation–fractional crystallization (EC-AFC) model to magmatic systems. *Journal of Petrology* **42**, 1019–1041.

Buchan, C., Cunningham, D., Windley, B. F. & Tomurhuu, D. (2001). Structural and lithological characteristics of the Bayankhongor ophiolite zone, Central Mongolia. *Journal of the Geological Society, London* **158**, 445–460.

Campbell, I. H. & Griffiths, R. W. (1990). Implications of mantle plume structure for the evolution of flood basalts. *Earth and Planetary Science Letters* **99**, 79–93.

Castillo, P. R., Natland, J. H., Niu, Y. L. & Lonsdale, P. F. (1998). Sr, Nd and Pb isotopic variation along the Pacific–Antarctic risecrest, 53–57° S: implications for the composition and dynamics of the South Pacific upper mantle. *Earth and Planetary Science Letters* **154**, 109–125.

Chauvel, C. & Blichert-Toft, J. (2001). A hafnium isotope and trace element perspective on melting of the depleted mantle. *Earth and Planetary Science Letters* **190**, 137–151.

Chung, S. L., Sun, S. S., Tu, K., Chen, C. H. & Lee, C. Y. (1994) Late Cenozoic basaltic volcanism around the Taiwan Strait, SE China—product of lithosphere–asthenosphere interaction during continental extension. *Chemical Geology* **112**, 1–20.

Class, C., Goldstein, S. L., Altherr, R. & Bachelery, P. (1998). The process of plume–lithosphere interactions in the ocean basins—the case of Grande Comore. *Journal of Petrology* **39**, 881–903.

Cobbold, P. R. & Davy, P. H. (1988). Indentation tectonics in nature and experiment. 2. Central Asia. *Bulletin of the Geological Institute, University of Uppsala* **14**, 143–162.

Cohen, R. S. & O'Nions, R. K. (1982). Identification of recycled continental material in the mantle from Sr, Nd and Pb isotope investigations. *Earth and Planetary Science Letters* **61**, 73–84.

Cunningham, W. D. (2001). Cenozoic normal faulting and regional doming in the southern Hangay region, Central Mongolia: implications for the origin of the Baikal rift province. *Tectonophysics* **331**, 389–411.

Cunningham, W. D., Windley, B. F., Owen, L. A., Barry, T., Dorjnamjaa, D. & Badamgarov, J. (1997). Geometry and style of partitioned deformation within a late Cenozoic transpressional zone in the eastern Gobi Altai Mountains, Mongolia. *Tectonophysics* **277**, 285–306.

Delvaux, D. (1997). Geodynamics of Baikal rifting: new developments and perspectives. *Geophysical Bulletin, Series D* **48**, 86–97.

DePaolo, D. J. (1981). Trace element and isotopic effects of combined wallrock assimilation and fractional crystallization. *Earth and Planetary Science Letters* **53**, 189–202.

Devyatkin, E. V. (1975). Neotectonic structures of western Mongolia. In: *Mesozoic and Cenozoic Tectonics and Magmatism of Mongolia.* Moscow: Nauka (in Russian).

Dosso, L., Bougault, H., Beuzart, P., Calvez, J.-Y. & Joron, J.-L. (1988). The geochemical structure of the South-east Indian Ridge. *Earth and Planetary Science Letters* **88**, 47–59.

Dupré, B., Lambret, B., Rousseau, D. & Allègre, C. J. (1981). Limitations on the scale of mantle heterogeneities under oceanic ridges. *Nature* **294**, 552–554.

Fan, Q. & Hooper, P. R. (1989). The mineral chemistry of ultramafic xenoliths from eastern China: implications for upper mantle composition and the paleogeotherm. *Journal of Petrology* **30**, 1117–1158.

Ferguson, E. M. & Klein, E. M. (1993). Fresh basalts from the Pacific Antarctic Ridge extend the Pacific geochemical province. *Nature* **366**, 330–333.

Fitton, J. G., Saunders, A. D., Larsen, L. M., Hardarson, B. S. & Norry, M. J. (1998). Volcanic rocks from the southeast Greenland margin at 63°N: composition, petrogenesis, and mantle sources. In: Saunders, A. D., Larsen, H. C. & Wise, S. W., Jr (eds). *Proceedings of the Ocean Drilling Program, Scientific Results* **152**, 331–350.

Flower, M. F. J., Zhang, M., Chen, C. Y., Tu, K. & Xie, G. H. (1992). Magmatism in the South China Basin. 2. Post-spreading Quaternary basalts from Hainan Island, South China. *Chemical Geology* **97**, 65–87.

Flower, M., Tamaki, K. & Hoang, N. (1998). Mantle extrusion: a model for dispersed volcanism and DUPAL-like asthenosphere in East Asia and the western Pacific. In: Flower, M., Chung, S.-L., Lo, C.-H. & Lee, T.-Y. (eds) *Mantle Dynamics and Plate Interactions in East Asia. American Geophysical Union Monograph, Geodynamics Series* **27**, 67–88.

Frey, F. A., Green, D. H. & Roy, S. D. (1978). Integrated models of basalt petrogenesis; a study of quartz tholeiites to olivine melilitites from Southeastern Australia utilizing geochemical and experimental petrological data. *Journal of Petrology* **19**, 463–513.

Genshaft, Y. S. & Saltykovskiy, A.Y. (1987). First kind of corundum megacrysts in Cenozoic basalts of Mongolia. *Doklady Akademii Nauk SSSR* **292**, 127–129.

Gibson, S. A., Thompson, R. N., Dickin, A. P. & Leonardos, O. H. (1995). High-Ti and low-Ti potassic magmas: key to plume–lithosphere interactions and continental flood-basalt genesis. *Earth and Planetary Science Letters* **136**, 149–165.

Greenough, J. D. (1988). Minor phases in the Earth's mantle: evidence from trace- and minor-element patterns in primitive alkaline magmas. *Chemical Geology* **69**, 177–192.

Hamelin, B. & Allègre, C. J. (1985). Large-scale regional units in the depleted upper mantle revealed by an isotope study of the South-West Indian Ridge. *Nature* **315**, 196–199.

Hamelin, B., Dupré, B. & Allègre, C. J. (1984). Lead–strontium isotopic variations along the East Pacific Rise and the Mid-Atlantic Ridge—a comparative study. *Earth and Planetary Science Letters* **67**, 340–350.

Hamelin, B., Dupré, B. & Allègre, C. J. (1986). Pb–Sr–Nd isotopic data of Indian Ocean ridges: new evidence of large-scale mapping of mantle heterogeneities. *Earth and Planetary Science Letters* **76**, 288–298.

Han, B.-F., Wang, S.-G. & Kagami, H. (1999). Trace element and Nd–Sr isotope constraints on origin of the Chifeng flood basalts, North China. *Chemical Geology* **155**, 187–199.

Hanan, B. B. & Schilling, J. G. (1989). Easter microplate evolution—Pb isotope evidence. *Journal of Geophysical Research* **94**, 7432–7448.

Hanson, G. N. & Langmuir, C. H. (1978). Modelling of major elements in mantle–melt systems using trace element approaches. *Geochimica et Cosmochimica Acta* **42**, 725–742.

Harmon, R., Kempton, P., Stosch, H., Hoefs, J., Kovalenko, V. & Ionov, D. (1987). $^{18}O/^{16}O$ ratios in anhydrous spinel lherzolite xenoliths from the Shavaryn-Tsaram volcano, Mongolia. *Earth and Planetary Science Letters* **81**, 193–202.

Hart, S. R. (1984). The DUPAL anomaly: a large-scale isotope anomaly in the southern hemisphere mantle. *Nature* **309**, 753–757.

Hart, S. R. & Dunn, T. (1993). Experimental cpx/melt partitioning of 24 trace elements. *Contributions to Mineralogy and Petrology* **113**, 1–8.

Hertogen, J. & Gijbels, R. (1976). Calculation of trace element fractionation during partial melting. *Geochimica et Cosmochimica Acta* **40**, 313–322.

Hickey-Vargas, R., Hergt, J. M. & Spadea, P. (1995). The Indian Ocean-type isotopic signature in Western Pacific marginal basins: origin and significance. *Geophysical Monograph, American Geophysical Union* **88**, 175–197.

Hoang, N. & Flower, M. (1998). Petrogenesis of Cenozoic basalts from Vietnam: implication for origins of a 'Diffuse igneous province'. *Journal of Petrology* **39**, 369–395.

Hofmann, A. W., Jochum, K. P., Seufert, M. & White, W. M. (1986). Nb and Pb in oceanic basalts: new constraints on mantle evolution. *Earth and Planetary Science Letters* **79**, 33–45.

Ionov, D. A. (1986). Spinel peridotite xenoliths from the Shavaryn-Tsaram volcano, northern Mongolia: petrography, major element chemistry and mineralogy. *Geologica Carpathica* **37**, 681–692.

Ionov, D. A. & Wood, B. J. (1992). The oxidation state of subcontinental mantle: oxygen thermobarometry of mantle xenoliths from central Asia. *Contributions to Mineralogy and Petrology* **111**, 179–193.

Ionov, D. A., Hoefs, J., Wedepohl, K. H. & Wiechert, U. (1992). Content and isotopic composition of sulphur in ultramafic xenoliths from Central Asia. *Earth and Planetary Science Letters* **111**, 269–286.

Ionov, D., Hofmann, A. & Shimizu, N. (1994). Metasomatism-induced melting in mantle xenoliths from Mongolia. *Journal of Petrology* **35**, 753–785.

Ionov, D. A., O'Reilly, S. Y. & Ashchepkov, I. V. (1995). Feldspar-bearing lherzolite xenoliths in alkali basalts from Hamar-Daban, southern Baikal region, Russia. *Contributions to Mineralogy and Petrology* **122**, 174–190.

Ionov, D. A., O'Reilly, S. Y. & Griffin, W. L. (1998). A geotherm and lithospheric section for Central Mongolia (Tariat region). In: Flower, M., Chung, S.-L., Lo, C.-H. & Lee, T.-Y. (eds) *Mantle Dynamics and Plate Interactions in East Asia. American Geophysical Union Monograph, Geodynamics Series* **27**, 127–153.

Ionov, D. A., Gregoire, M. & Prikhod'ko, V. S. (1999). Feldspar–Ti-oxide metasomatism in off-cratonic continental and oceanic upper mantle. *Earth and Planetary Science Letters* **165**, 37–44.

Ito, E., White, W. M. & Gopel, C. (1987). The O, Sr, Nd and Pb isotope geochemistry of MORB. *Chemical Geology* **62**, 157–176.

Johnson, C. M. & Beard, B. L. (1993). Evidence from hafnium isotopes for ancient sub-oceanic mantle beneath the Rio Grande Rift. *Nature* **362**, 441–444.

Kempton, P. D. (1995). Common Pb chemical procedures for silicate rocks and minerals, methods of data correction and an assessment of data quality at the NERC Isotope Geosciences Laboratory. *NIGL Report Series No. 78*, 26 pp.

Kempton, P. D., Dungan, M. A. & Blanchard, D. P. (1987). Petrology and geochemistry of xenolith-bearing alkalic basalts from the Geronimo Volcanic Field, S.E. Arizona: evidence for polybaric fractionation and implications for mantle heterogeneity. In: Morris, E. M. & Pasteris, J. D. (eds) *Mantle Metasomatism and Alkaline Magmatism. Geological Society of America, Special Papers* **215**, 347–370.

Kempton, P. D., Fitton, J. G., Hawkesworth, C. J. & Ormerod, D. S. (1991). Isotopic and trace element constraints on the composition and evolution of the lithosphere beneath the southwestern United States. *Journal of Geophysical Research* **96**, 13713–13735.

Kempton, P. D., Pearce, J. A., Barry, T. L., Fitton, J. G., Langmuir, C. & Christie, D. M. (2002). Sr–Nd–Pb–Hf isotope results from ODP Leg 187: evidence for mantle dynamics of the Australian–Antarctic discordance and origin of the Indian MORB source. *Geochemistry, Geophysics, Geosystems (G^3)* (in press).

Kepezhinskas, V. V. (1979). Cenozoic alkaline basaltoids of Mongolia and related deep inclusions. *Doklady Akademii Nauk SSSR* **25**, 1–312.

Khain, V. E. (1990). Origin of the Central Asian mountain belt: collision or mantle diapirism. *Journal of Geodynamics* **11**, 389–394.

Khutorskoy, M. & Yarmoluk, V. (1989). Heat flow, structure and evolution of the lithosphere of Mongolia. *Tectonophysics* **164**, 315–322.

Kiselev, A. I. (1985). Tectonophysical conditions of basalt volcanism in the Baikal Rift Zone. *Doklady Akademii Nauk SSSR* **274**, 62–65.

Klein, E. M., Langmuir, C. H., Zindler, A., Staudigel, H. & Hamelin, B. (1988). Isotope evidence of a mantle convection boundary at the Australian–Antarctic discordance. *Nature* **333**, 623–629.

Kopylova, M. G., Genshaft, Y. S. & Saltykovskiy, A. Y. (1990). Garnet–spinel rocks in the Cenozoic basalts of Mongolia. *Doklady Akademii Nauk SSSR* **312**, 165–168.

Kopylova, M. G., O'Reilly, S. Y. & Genshaft, Y. S. (1995). Thermal state of the lithosphere beneath Central Mongolia: evidence from deep-seated xenoliths from the Shavaryn-Saram volcanic centre in the Tariat depression, Hangai, Mongolia. *Lithos* **36**, 243–255.

Kovalenko, V. I., Yarmolyuk, V. V., Ionov, D. A., Jagoutz, E., Lugmair, G. W. & Stosch, H.-G. (1990). Mantle evolution in central Asia and development of tectonic structures of the earth's crust. *Geotectonics* **24**, 283–292.

Kozhevnikov, V. M. (1999). Rayleigh wave group velocity tomography and S-waves velocities distribution in the Earth's crust and upper mantle of Central Asia. 3rd Annual Meeting of IGCP 400 (Baikal), unpublished abstract volume.

Langmuir, C. H., Bender, J. F., Bence, A. E. & Hanson, G. N. (1977). Petrogenesis of basalts from the Famous area: mid-Atlantic ridge. *Earth and Planetary Science Letters* **36**, 133–156.

La Tourrette, T., Hervig, R. L. & Holloway, J. R. (1995). Trace element partitioning between amphibole, phlogopite, and basanite melt. *Earth and Planetary Science Letters* **35**, 13–30.

Le Bas, M., Le Maitre, R., Streckeisen, A. & Zanettin, B. (1986). A chemical classification of volcanic rocks based on the total alkali–silica diagram. *Journal of Petrology* **27**, 745–750.

Litasov, K. D., Foley, S. F. & Litasov, Y. D. (2000). Magmatic modification and metasomatism of the subcontinental mantle beneath the Vitim volcanic field (East Siberia): evidence from trace element data on pyroxenite and peridotite xenoliths from Miocene picrobasalt. *Lithos* **54**, 83–114.

Logatchev, N. A. (1984). The Baikal Rift system. *Episodes* **7**, 38–43.

Lysak, S. (1995). Terrestrial heat and temperatures in the upper crust in South East Siberia. *Bulletin des Centres de Recherches Exploration–Production Elf Aquitaine* **19**, 39–58.

MacDougall, J. D. & Lugmair, G. W. (1986). Sr and Nd isotopes in basalts from the East Pacific Rise—significance for mantle heterogeneity. *Earth and Planetary Science Letters* **77**, 273–284.

Mahoney, J. J., Natland, J. H., White, W. M., Poreda, R., Bloomer, S. H., Fisher, R. L. & Baxter, A. N. (1989). Isotopic and geochemical provinces of the Western Indian Ocean spreading centers. *Journal of Geophysical Research* **94**, 4033–4052.

Mahoney, J., LeRoex, A. P., Peng, Z., Fisher, R. L. & Natland, J. H. (1992). Southwestern limits of Indian Ocean ridge mantle and the origin of low $^{206}Pb/^{204}Pb$ mid-ocean ridge basalts: isotope systematics of the central southwest Indian ridge (17–50°E). *Journal of Geophysical Research* **97**, 19771–19790.

Mahoney, J. J., Sinton, J. M., Kurz, M. D., Macdougall, J. D., Spencer, K. J. & Lugmair, G. W. (1994). Isotope and trace-element characteristics of a super-fast spreading ridge—East Pacific Rise, 13–23°S. *Earth and Planetary Science Letters* **121**, 173–193.

Mahoney, J. J., White, W. M., Upton, B. G. J., Neal, C. R. & Scrutton, R. A. (1996). Beyond EM-1: lavas from Afanasy-Nikitin Rise and the Crozet Archepelago, Indian Ocean. *Geology* **24**, 615–618.

McKenzie, D. & Bickle, M. J. (1988). The volume and composition of melt generated by extension of the lithosphere. *Journal of Petrology* **29**, 625–679.

McKenzie, D. & O'Nions, R. K. (1991). Partial melt distributions from inversion of rare earth element concentrations. *Journal of Petrology* **32**, 1021–1091.

McKenzie, D. & O'Nions, R. K. (1995). The source regions of ocean island basalts. *Journal of Petrology* **36**, 133–159.

Mengel, K. & Green, D. H. (1989). Stability of amphibole and phlogopite in metasomatised peridotite under water-saturated and water-undersaturated conditions. In: Ross, J. (ed.) *Fourth International Kimberlite Conference. Geological Society of Australia Special Publication* **14**, 571–581.

Menzies, M. A., Fan, W. & Zhang, M. (1993). Palaeozoic and Cenozoic lithoprobes and the loss of >120 km of Archaean lithosphere, Sino-Korean craton, China. In: Pritchard, H. M., Alabaster, T., Harris, N. B. W. & Neary, C. R. (eds) *Magmatic Processes and Plate Tectonics. Geological Society, London, Special Publications* **76**, 71–81.

Michard, A., Montigny, R. & Schlich, R. (1986). Geochemistry of the mantle beneath the Rodriguez Triple Junction and the South-east Indian Ridge. *Earth and Planetary Science Letters* **78**, 104–114.

Navon, O. & Stolper, E. (1987). Geochemical consequences of melt percolation: the upper mantle as a chromatographic column. *Journal of Geology* **95**, 285–307.

Nguyen, H., Flower, M. F. J. & Carlson, R. W. (1996). Major, trace element, and isotopic compositions of Vietnamese basalts: interaction of hydrous EM1-rich asthenosphere with thinned Eurasian lithosphere. *Geochimica et Cosmochimica Acta* **60**, 4329–4351.

Niu, Y. L., Waggoner, D. G., Sinton, J. M. & Mahoney, J. J. (1996). Mantle source heterogeneity and melting processes beneath seafloor spreading centers: the East Pacific Rise, 18–19°S. *Journal of Geophysical Research* **101**, 27711–27733.

Nowell, G. M., Kempton, P. D., Noble, S. R., Fitton, J. G., Saunders, A. D., Mahoney, J. J. & Taylor, R. N. (1998*a*). High precision Hf isotope measurements of MORB and OIB by thermal ionisation

mass spectrometry: insights into the depleted mantle. *Chemical Geology* **149**, 211–233.

Nowell, G. M., Pearson, D. G. & Kempton, P. D. (1999). Hafnium-isotopic systematics of kimberlites, lamproites, and megacrysts: implications for mantle reservoirs and the composition of bulk silicate Earth. Ninth Annual V. M. Goldschmidt Conference, Cambridge, Massachusetts. *Lunar and Planetary Institute Contribution* **971**, 211–212.

O'Reilly, S. Y. & Zhang, M. (1995). Geochemical characteristics of lava-field basalts from eastern Australia and inferred sources: connections with the subcontinental lithospheric mantle? *Contributions to Mineralogy and Petrology* **121**, 148–170.

Pearce, J. A., Kempton, P. D., Nowell, G. M. & Noble, S. R. (1999). Hf–Nd element and isotope perspective on the nature and provenance of mantle and subduction components in western Pacific arc–basin systems. *Journal of Petrology* **40**, 1579–1611.

Peate, D. W. & Hawkesworth, C. J. (1996). Lithospheric to asthenospheric transition in low-Ti flood basalts from southern Parana, Brazil. *Chemical Geology* **127**, 1–24.

Petit, C., Deverchere, J., Calais, E., San'kov, V. & Fairhead, D. (2002). Deep structure and mechanical behaviour of the lithosphere in the Hangai–Hovsgol region, Mongolia: new constraints from gravity modelling. *Earth and Planetary Science Letters* **197**, 133–149.

Pik, R., Deniel, C., Coulon, C., Yirgu, G., Hofmann, C. & Ayalew, D. (1998). The northwestern Ethiopian Plateau flood basalts: classification and spatial distribution of magma types. *Journal of Volcanology and Geothermal Research* **81**, 91–111.

Pik, R., Deniel, C., Coulon, C., Yirgu, G. & Marty, B. (1999). Isotopic and trace element signatures of Ethiopian flood basalts: evidence for plume–lithosphere interactions. *Geochimica et Cosmochimica Acta* **63**, 2263–2279.

Preß, S., Witt, G., Seck, H. A., Ionov, D. & Kovalenko, V. I. (1986). Spinel peridotite xenoliths from the Tariat Depression, Mongolia. I: Major element chemistry and mineralogy of a primitive mantle xenolith suite. *Geochimica et Cosmochimica Acta* **50**, 2587–2599.

Price, R. C., Kennedy, A. K., Riggs-Sneeringer, M. & Frey, F. A. (1986). Geochemistry of basalts from the Indian ocean triple junction: implications for the generation and evolution of Indian ocean ridge basalts. *Earth and Planetary Science Letters* **78**, 279–296.

Pyle, D. G., Christie, D. M. & Mahoney, J. J. (1992). Resolving an isotopic boundary within the Australian–Antarctic discordance. *Earth and Planetary Science Letters* **112**, 161–178.

Rehkämper, M. & Hofmann, A. W. (1997). Recycled ocean crust and sediment in Indian Ocean MORB. *Earth and Planetary Science Letters* **147**, 93–106.

Rollinson, H. R. (1993). *Using Geochemical Data; Evaluation, Presentation, Interpretation*. Harlow: Longman, 352 pp.

Royse, K. R., Kempton, P. D. & Darbyshire, D. P. F. (1998). Procedure for the analysis for rubidium–strontium and samarium–neodymium isotopes at the NERC Isotope Geosciences Laboratory. *NIGL Report Series No. 121*, 28 pp.

Salters, V. J. M. & Hart, S. R. (1991). The mantle sources of ocean ridges, islands and arcs—the Hf-isotope connection. *Earth and Planetary Science Letters* **104**, 364–380.

Schiano, P., Birck, J. L. & Allègre, C. J. (1997). Osmium–strontium–neodymium–lead isotopic covariations in mid-ocean ridge basalt glasses and the heterogeneity of the upper mantle. *Earth and Planetary Science Letters* **150**, 363–379.

Sengör, A. M. C. & Natal'in, B. A. (1996). Paleotectonics of Asia fragments of a synthesis. In: Yin, A. & Harrison, M. (eds) *Tectonic Evolution of Asia*. Cambridge: Cambridge University Press, pp. 486–640.

Song, Y., Frey, F. A. & Zhi, X. (1990). Isotopic characteristics of Hannuoba basalts, eastern China: implications for their petrogenesis and the composition of the subcontinental mantle. *Chemical Geology* **88**, 35–52.

Stimac, J. A. & Hickmott, D. (1994). Trace-element partition coefficients for ilmenite, orthopyroxene and pyrrhotite in rhyolite determined by micro-PIXE analysis. *Chemical Geology* **117**, 313–330.

Storey, M., Saunders, A. D., Tarney, J., Leat, P., Thirlwall, M. F., Thompson, R. N., Menzies, M. A. & Marriner, G. F. (1988). Geochemical evidence for plume–mantle interactions beneath Kerguelen and Heard Islands, Indian Ocean. *Nature* **336**, 371–374.

Stosch, H.-G. (1987). Constitution and evolution of subcontinental upper mantle and lower crust in areas of young volcanism: differences and similarities between the Eifel (F. R. Germany) and Tariat Depression (central Mongolia) as evidenced by peridotite and granulite xenoliths. *Fortschritte der Mineralogie* **65**, 49–86.

Stosch, H., Lugmair, G. & Kovalenko, V. (1986). Spinel peridotite xenoliths from the Tariat Depression, Mongolia. II: geochemistry and Nd and Sr isotopic composition and their implications for the evolution of the subcontinental lithosphere. *Geochimica et Cosmochimica Acta* **50**, 2601–2614.

Stosch, H.-G., Ionov, D. A., Puchtel, I. S., Galer, S. J. G. & Sharpouri, A. (1995). Lower crustal xenoliths from Mongolia and their bearing on the nature of the deep crust beneath central Asia. *Lithos* **36**, 227–242.

Sun, S. & McDonough, W. F. (1989). Chemical and isotope systematics of oceanic basalts: implications for mantle composition and processes. In: Saunders, A. D. & Norry, M. J. (eds) *Magmatism in the Ocean Basins. Geological Society, London, Special Publications* **42**, 313–345.

Tainton, K. M. & McKenzie, D. (1994). The generation of kimberlites, lamproites, and their source rocks. *Journal of Petrology* **35**, 787–817.

Tapponnier, P. & Molnar, P. (1979). Active faulting and Cenozoic tectonics of the Tien Shan, Mongolia, and Baykal Regions. *Journal of Geophysical Research* **84**, 3425–3459.

Tatsumoto, M., Basu, A. R., Wankang, H., Junwen, W. & Guanghong, X. (1992). Sr, Nd and Pb isotopes in ultramafic xenoliths in volcanic rocks of eastern China: enriched components EMI and EMII in sub-continental lithosphere. *Earth and Planetary Science Letters* **113**, 107–128.

Taylor, S. R. & McClennan, S. M. (1985). *The Continental Crust: its Composition and Evolution*. Oxford: Blackwell, 312 pp.

Thompson, R. N. (1974). Primary basalts and magma genesis. *Contributions to Mineralogy and Petrology* **45**, 317–341.

Thompson, R. N. & Gibson, S. A. (1991). Subcontinental mantle plumes, hotspots and pre-existing thinspots. *Journal of the Geological Society, London* **148**, 973–977.

Tiepolo, M., Vannucci, R., Oberti, R., Foley, S., Bottazzi, P. & Zanetti, A. (2000). Nb and Ta incorporation and fractionation in titanian pargasite and kaersutite: crystal-chemical constraints and implications for natural systems. *Earth and Planetary Science Letters* **176**, 185–201.

Todt, W., Cliff, V., Hanser, A. & Hofmann, A. W. (1993). Recalibration of NBS Pb standards using a $^{202}Pb + {}^{205}Pb$ double spike. *Terra Nova* **5**, *Terra Abstracts Supplement 1*, 396.

Tu, K., Flower, M. F. J., Carlson, R. W., Xie, G. H., Chen, C. Y. & Zhang, M. (1992). Magmatism in the South China Basin. 1. Isotopic and trace-element evidence for an endogenous Dupal mantle component. *Chemical Geology* **97**, 47–63.

Vervoort, J. D. & Blichert-Toft, J. (1999). Evolution of the depleted mantle: Hf isotope evidence from juvenile rocks through time. *Geochimica et Cosmochimica Acta* **63**, 533–556.

Vlastélic, I., Aslanian, D., Dosso, L., Bougault, H., Olivet, J. L. & Geli, L. (1999). Large-scale chemical and thermal division of the Pacific mantle. *Nature* **399**, 345–350.

Villaseñor, A., Ritzwoller, M. H., Levshin, A. L., Barmin, M. P., Engdahl, E. R., Spakman, W. & Trampert, J. (2001). Shear velocity structure of central Eurasia from inversion of surface wave velocities. *Physics of the Earth and Planetary Interiors* **123**, 169–184.

White, W. M. & Hofmann, A. W. (1982). Sr and Nd isotope geochemistry of oceanic basalts and mantle evolution. *Nature* **296**, 821–825.

White, W. M., Hofmann, A. W. & Puchelt, H. (1987). Isotope geochemistry of Pacific mid-ocean ridge basalt. *Journal of Geophysical Research* **92**, 4881–4893.

Whitford-Stark, J. L. (1987). *A Survey of Cenozoic Volcanism on Mainland Asia. Geological Society of America, Special Papers* **213**, 74 pp.

Wiechert, U., Ionov, D. A. & Wedepohl, K. H. (1997). Spinel peridotite xenoliths from the Atsagin-Dush volcano, Dariganga lava plateau, Mongolia: a record of partial melting and cryptic metasomatism in the upper mantle. *Contributions to Mineralogy and Petrology* **126**, 345–364.

Wilson, M. & Downes, H. (1991). Tertiary–Quaternary extension-related alkaline magmatism in Western and Central Europe. *Journal of Petrology* **32**, 811–849.

Wilson, M. & Patterson, R. (2001). Intraplate magmatism related to short-wavelength convective instabilities in the upper mantle: evidence from the Tertiary–Quaternary volcanic province of western and central Europe. *Geological Society of America, Special Papers* **352**, 37–58.

Wilson, M., Rosenbaum, J. M. & Dunworth, E. A. (1995). Melilitites: partial melts of the thermal boundary layer. *Contributions to Mineralogy and Petrology* **119**, 181–196.

Windley, B. F. & Allen, M. B. (1993). Mongolian plateau: evidence for a late Cenozoic mantle plume under central Asia. *Geology* **21**, 295–298.

Yarmolyuk, V. V., Kovalenko, V. I. & Samoylov, V. S. (1991). Tectonic setting of late Cenozoic volcanism of Central Asia. *Geotectonics* **25**, 53–63.

Zhang, M., O'Reilly, S. Y. & Chen, D. G. (1999). Location of Pacific and Indian mid-ocean ridge-type mantle in two time slices: evidence from Pb, Sr, and Nd isotopes for Cenozoic Australian basalts. *Geology* **27**, 39–42.

Zindler, A. & Hart, S. R. (1986). Chemical geodynamics. *Annual Review of Earth and Planetary Sciences* **14**, 493–571.

Zorin, Y. A. (1981). The Baikal rift: an example of the intrusion of asthenospheric material into the lithosphere as the cause of disruption of lithospheric plates. *Tectonophysics* **73**, 91–104.

Zorin, Y. A. & Lepina, S. V. (1985). Geothermal aspects of development of asthenospheric upwellings beneath continental rift zones. *Journal of Geodynamics* **3**, 1–22.

APPENDIX: ANALYTICAL METHODS

ICP-AES (Leicester): total digestion

Concentrated HNO_3 (2·0 ml) was added to 0·1 g of sample weighed into a clean PTFE test-tube. After leaving the test-tubes in a hot-block overnight at 50°C, 1·0 ml of 60% $HClO_4$ + 5·0 ml 48% HF were added, and the tubes were returned to the hot-block for 3 h at 100°C. This was followed by 3 h at 140°C and 6 h at 190°C until dry. After removing the tubes and allowing them to cool, 1·0 ml of concentrated HCl was added and mixed thoroughly. The tubes were heated for 1 h at 50°C, and then allowed to cool. Each sample was diluted with 10 ml deionized H_2O, and mixed thoroughly, ready for centrifuging before analysis.

ICP-AES (Leicester): REE analysis

Sample (0·5 g) was weighed into a 50 ml PTFE beaker and dampened with de-ionized H_2O, followed by the addition of 15 ml of 40% HF to each beaker, plus 4 ml 60–70% $HClO_4$. The beakers were then dried on a hotplate at 180–200°C. Once dry, a further 4 ml $HClO_4$ was added and mixed thoroughly, before drying again. HCl (30 ml, 1·7N) was added to each beaker and warmed until the sample had completely dissolved, after which the sample was transferred to a clean Pyrex beaker ready for separation.

For REE separation, glass columns of 180 mm length × 8 mm diameter were used. The columns had 100 ml reservoirs at the top and quartz glass wool at the bottom. Five grams of Dowex AG 50W-8X, 200–400 mesh resin was loaded onto the columns in 1·7N HCl and settled to a height of 130 mm. The resin was washed with 50 ml 6M HCl, 50 ml de-ionized H_2O and 50 ml 1·7N HCl. The samples were loaded in 30 ml 1·7N HCl, and allowed to elute. After a further 100 ml elution of 1·7N HCl to remove major elements, the REE fraction was collected in 100 ml Pyrex beakers with 80 ml 6M HCl. This was evaporated to dryness on a sand bath at 110°C and when dry, 4 ml 16M HNO_3 was added and the sample was dried again. Each sample can be redissolved in 3 ml 5% HNO_3, in readiness for analysis. A blank and standard were run with each batch.